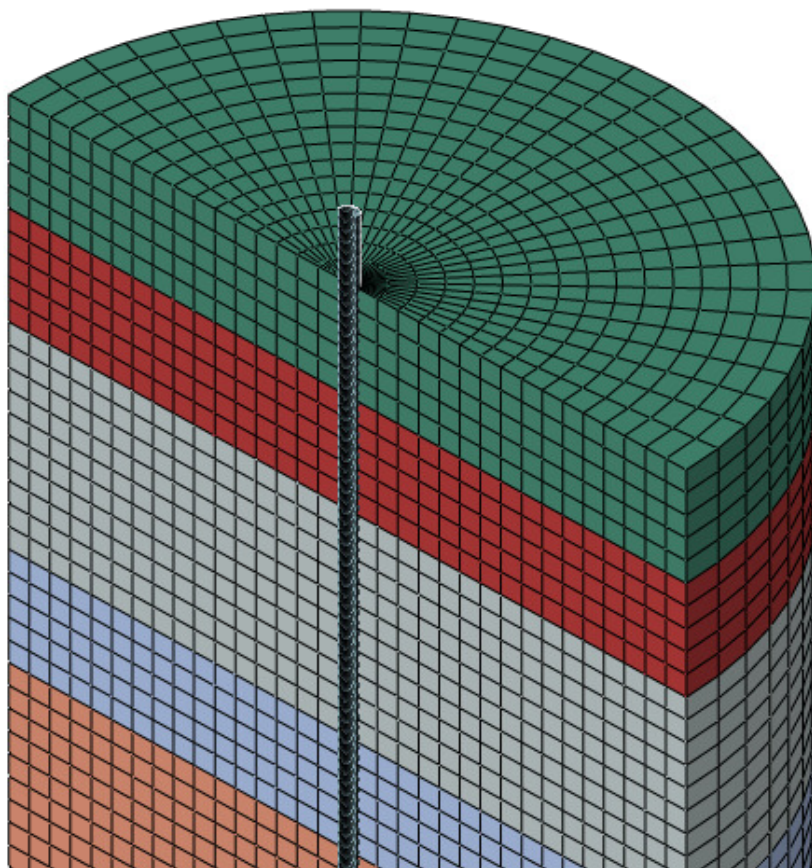# CHALMERS

Modeling of Soil and Structure Interaction Subsea
Master's thesis in Applied Mechanics

NICHOLAS STRÖMBLAD

Department of Applied Mechanics
Division of Material and Computational Mechanics
CHALMERS UNIVERSITY OF TECHNOLOGY
Göteborg, Sweden 2014
Master's thesis 2014:09

Modeling of Soil and Structure Interaction Subsea

NICHOLAS STRÖMBLAD

Department of Applied Mechanics
Division of Material and Computational Mechanics
CHALMERS UNIVERSITY OF TECHNOLOGY

Göteborg, Sweden 2014

Cover:
Mesh of a wellhead and a surrounding layered soil

Modeling of Soil and Structure Interaction Subsea
Master's thesis in Applied Mechanics
NICHOLAS STRÖMBLAD
Department of Applied Mechanics
Division of Material and Computational Mechanics
Chalmers University of Technology

Abstract

The mechanical behavior of structures that are in contact with soil is affected by the interaction between the soil and the structure. This interaction is called Soil-Structure Interaction, abbreviated SSI. Some structures where SSI is especially important are buildings, bridges and oil rigs. In this thesis a laterally loaded component of an offshore oil rig has been studied, and in particular how to model the soil to best capture the interaction with the soil. The component is located in the sea bed, meaning that the interacting soil is completely submerged.

A simple and conventional approach is to model the soil using lateral non-linear springs, where the behavior of the springs is dependent on soil type, soil properties, loading and depth below sea bed. It is a widely accepted method in geotechnical engineering, but the one-dimensional springs suffer from certain limitations and an alternative modeling strategy is needed to truly capture the complex three-dimensional behavior of soils, such as modeling the soil as a continuum with solid elements.

In this thesis a literature study was carried out to understand the mechanical behavior of soils, and especially the method used to determine the behavior of the non-linear springs. Then, a finite element model of the specific component and the surrounding soil was created in Abaqus/CAE, for three different soil compositions. The soil was modeled both with non-linear springs and as a continuum, and the results from the two modeling strategies were compared, along with identification of limitations and benefits for the two approaches.

For the static load case studied it can be concluded that the results are similar, but there are also some notable differences mainly dependent on soil composition and material properties. Continuum soil modeling is more complex and computationally expensive than non-linear springs modeling, but is advantageous in prediction of long-term effects.

Future work should focus on determination of a soil's properties, as these highly influence the results for both modeling strategies. With an accurate characterization of a soil's behavior, the response of the structure will be predicted as correctly as possible.

Keywords: soil-structure interaction, soil mechanics, finite element method, non-linear springs, continuum soil, $P - y$ curves, subsea, wellhead, Abaqus

Preface

This Master's thesis addresses the interaction between a structure located in the sea bed and the surrounding soil, an interaction commonly known as Soil-Structure Interaction (SSI). The thesis is part of the Master's programme *Applied Mechanics* at Chalmers University of Technology in Gothenburg and was carried out during the first half of 2014 (30 higher education credits). The work was carried out in collaboration with ÅF and Aker Solutions, at the ÅF office situated in Gothenburg.

Acknowledgements

Nomenclature

Roman upper case letters

D	Diameter	[m]
E	Young's modulus	[Pa]
G_s	Specific gravity	[-]
I	Second moment of area	[m^4]
M	Bending moment	[Nm]
P	(Lateral) soil resistance	[N/m]
S	Degree of saturation	[-]
T	Transverse load	[N]
V	Volume	[m^3]
W	Weight	[N]
X	Depth below sea bed	[m]

Roman lower case letters

c	Cohesion	[Pa]
e	Void ratio	[-]
g	Acceleration of gravity	[m/s^2]
k	Initial soil modulus	[Pa/m]
m	Mass	[kg]
n	Porosity	[-]
p	Pore water pressure	[Pa]
s	Shear strength	[Pa]
y	Lateral deflection	[m]

Greek lower case letters

γ	Unit weight	[N/m^3]
ϵ	Strain	[-]
μ	Coefficient of friction	[-]
ν	Poisson's ratio	[-]
ρ	Density	[kg/m^3]
σ	Stress	[Pa]
τ	Shear stress	[Pa]
φ	Friction angle	[°]
ψ	Angle of dilation	[°]

CONTENTS

1 Introduction

1.1 Background

Subsea structures in the offshore industry are often in contact with the surrounding soil. Therefore, the behavior of the structure is dependent on both the structure itself and the soil. This phenomenon is called Soil-Structure Interaction (SSI) and is often neglected when analyzing subsea structures. However, for heavy structures resting on relatively soft soil the effects of SSI become prominent according to [1].

In this thesis a specific subsea component within oil and gas production systems is studied. An schematic overview of an oil rig is shown in Figure 1.1.
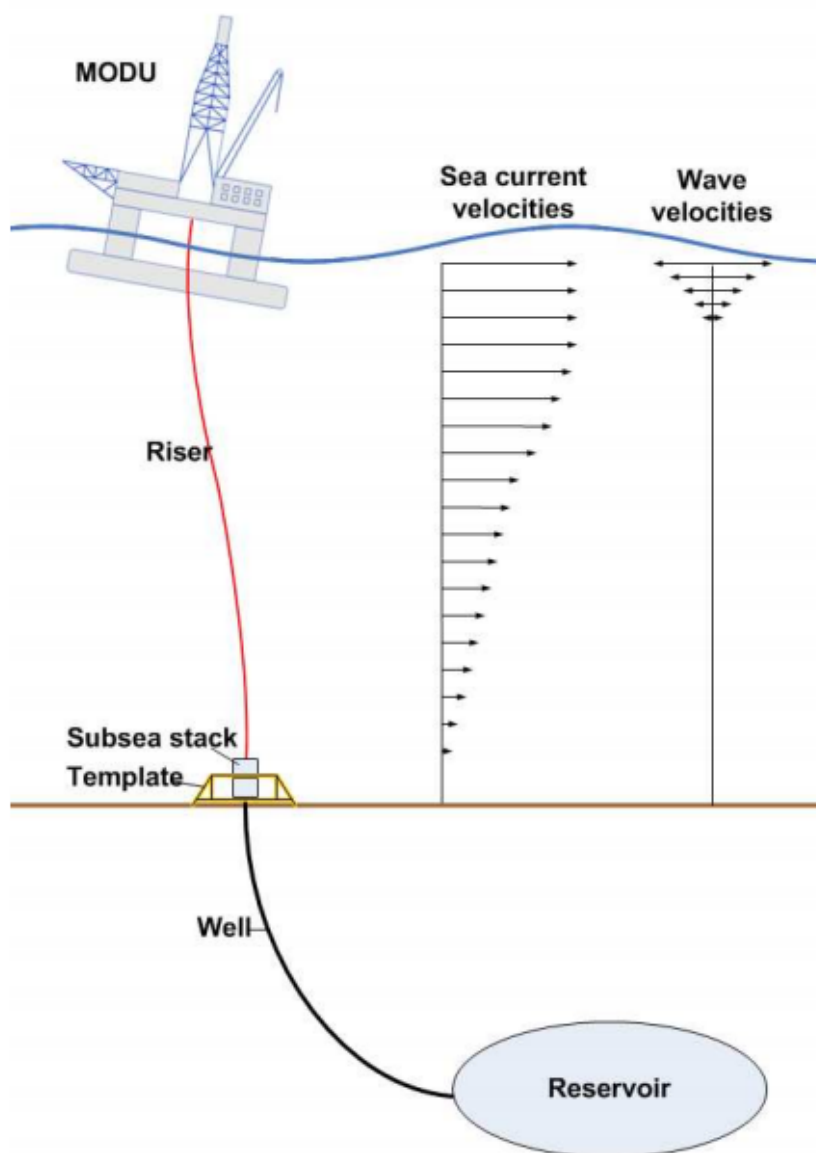

Figure 1.1: *Overview of an offshore oil rig, from [2]*

A Mobile Offshore Drilling Unit (MODU) is connected via a riser to a template at the sea bed, where a well to the oil reservoir is drilled. A specific part of the well is the wellhead assembly, which consists of a wellhead, housings, casings, connectors and several other minor components. Figure 1.2 shows a typical wellhead assembly.
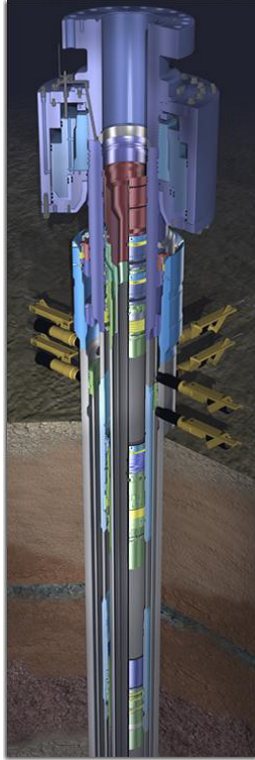
Figure 1.2: *Wellhead assembly and surrounding soil*

The wellhead assembly is subjected to lateral structural loads but also to hydrodynamic loads such as currents and waves. Due to the movement of the MODU, the wellhead assembly is subjected to high cyclic lateral loading and subsequently the deformation of the soil becomes substantial. As a result, the interaction between the surrounding soil and the wellhead becomes significant. Because of the cyclic loads, a fatigue analysis of the wellhead assembly is in general necessary to do and a recommended method is described in [2]. Especially important in the fatigue analysis is the interaction between the soil and the wellhead assembly. The specific component studied in this thesis is the wellhead itself and can be described as a vertical pipe.

A conventional method to model the soil is to use one-dimensional non-linear springs with $P - y$ curves. The lateral soil resistance P is related to the lateral soil deflection y, which is a non-linear relationship dependent on many factors, such as the soil type and strength of the soil, cf. [2]. Guidelines for constructing $P - y$ curves exist in literature and empirical formulas are commonly used. However, many different formulas have been suggested and it does not exist any general formulation applicable to all different types of soil. As an alternative, it is proposed to perform full-scale tests of soil samples to obtain as credible properties as possible and subsequently a $P - y$ curve reflecting the lateral relationship in a realistic way, as mentioned in [3].

In reality soil behavior is three-dimensional, which is not accounted for in the one-dimensional $P - y$ curves. Combined with the uncertainties present in the $P - y$ curves, a different model strategy is needed. One approach would be to model the soil as a continuum in a commercial software, e.g. Abaqus/CAE. There are numerous softwares available, see [4], but regardless of the software used, a proper model of the soil must be employed, in which the soil's properties and behavior are taken into account in a realistic way.

1.2   Purpose

The main purpose of this thesis is to identify different modeling strategies for soil and compare these. As mentioned above, a conventional way to model the soil is by utilizing $P - y$ curves. Another suitable method to model the soil will be identified and the limitations of the two modeling strategies is to be determined.

A secondary purpose is to, via this thesis, strengthen ÅF's competence in soil-structure interaction and open up the possibility for future projects in this field.

1.3   Method

In this section the method is briefly presented. It can be divided into the following steps:

- Carry out a literature study to gain knowledge about SSI and specifically $P - y$ curves, focusing on the method used to define them

- Build a 3D model of the wellhead, model the soil with non-linear springs using $P - y$ curves and finding an optimal discretization of the springs to obtain realistic results

- Model the soil as a continuum using solid elements and compare the response to the non-linear springs model

- Identify limitations/benefits for the two modeling strategies

1.4   Limitations

For the thesis work, the following limitations were identified:

- No studies about soil material parameters and how they are determined will be carried out, it is presumed that the material parameters are known beforehand

- Other soils than clay or sand will not be taken into consideration

- No other commercial software than Abaqus will be used

- Only static loading will be considered to get a first estimation and understanding of the soil-structure interaction

- When modeling the soil as a continuum, only the finite element method and solid elements will be considered

2 Soil mechanics

It is important to understand how soil reacts when subjected to loading and what type of parameters that defines a certain soil. Before resorting to finite element modeling, some basic soil mechanics will be presented together with the conventional non-linear $P - y$ relationship.

2.1 Definition

According to [5], soil is the product of physical and chemical weathering of rocks. Soils are located in the earth's crust and the non-weathered material is denoted rock with its behavior being determined by rock mechanics. A typical feature of a soil is that it is possible to dig a trench in the soil with simple tools or even by hand, whereas this is impossible for rock. Soil is a natural material, created by various geological processes throughout history, meaning that each soil is in fact unique. Three components are usually present in a soil: solid particles, liquid and gas, cf. [5].

There are many different types of soil and also numerous different systems of soil classification due to local variations and characteristics. However, one internationally agreed terminology is based on the grain size of the soil solid particles, according to [6]. The different soil types and their respective grain sizes is shown in Table 2.1.

Table 2.1: Soil types and grain sizes, modified from [6]

	Grain size [mm]	
Soil type	Minimum	Maximum
Clay		0.002
Silt	0.002	0.063
Sand	0.063	2
Gravel	2	63

Materials with larger particles than 63 mm are denoted stones. The four soil types exhibit rather different mechanical behavior and the grain size is useful to categorize the soil but not to predict the mechanical properties, as stated in [6]. Soils of the same grain size may have different mechanical properties and these must be determined from mechanical tests.

2.2 Behavior

The nature of soils is different from traditional materials such as steel or concrete, where the mechanical behavior can be considered linear if the deformations are not too large. The mechanical properties of soils are often strongly non-linear, with irreversible plastic deformations during loading and unloading. Additionally, soils usually show anisotropic behavior, creep and dilatancy, where the latter is a volume change during shear, as stated in [7]. Because of the inhomogeneous structure of soils, the mechanical behavior is hard to predict. Assuming a linear or piece-wise linear response can only give an approximate response and a constitutive model for the inelastic behavior is generally needed, cf. [8]. To further complicate the behavior of soils, there may exist water in the pores, giving rise to a pore water pressure within the soil.

A special property of soils is that the stiffness and strength of the soil increases when subjected to compressive stresses. This is due to the fact that when compressed, the forces between the individual soil particles increase, which in turn leads to an increased strength, cf. [5].

In shear however, soils become softer. If the shear stresses reach a certain level, failure will occur and soils generally fail in shear, as stated in [9]. For example, a sand pile cannot have a slope larger than about 35° and at greater slopes the particles would slide over each other, and failure occurs. This is a typical failure mechanism that has occurred all over the world, as mentioned in [6]. A steep slope is possible for fine soils, such as clay, for a limited period of time.

When a soil is subjected to shear, a volume change usually occurs, called dilatancy. For example, very loose sand has a tendency to contract during shear whereas dense sand undergoes a volume expansion. This is due to the fact that the particles shear over each other. Fine soils with small grain sizes such as clay, show little or none dilatancy, cf. [9].

Creep is another phenomenon of interest when studying soils, which means that the deformations are dependent upon time. Clay is a soil type which is particularly influenced by creep and this must be taken into account when, for example, predicting the settlement of a building over a period of time. If the settlement is not uniform, the building may be damaged, cf. [6]. At normal stress levels, sand shows in principle no creep.

Soil is a porous material consisting of a grain skeleton with pores. If there is a fluid present in the pores, it contributes to the stress transfer in the soil. Often the fluid is water and the pressure in this water is called pore pressure, according to [5]. In analyses of soil stresses, a common approach is to divide the stress into an effective stress and a pore pressure, meaning that the total stress is the sum of the two quantities. However, this applies only to the normal stresses, as the pores are not able to transfer shear stresses, as stated in [6].

It cannot be stressed enough that soil is a natural material created by various geological processes. Therefore the mechanical properties can be hard to predict via desk studies as the complete geological history is often unknown. For an accurate prediction of the mechanical behavior of a certain soil, the engineer should resort to laboratory or field testing, cf. [9].

2.3   Concepts and material parameters

Because of the complex behavior of soils under loading, the applicability range of a certain parameter is restricted to a limited set of problems. To find a soil's properties, nothing can beat experimental results, either in situ (in the field) or in the laboratory, as mentioned in [9]. Subsequently, in engineering practice the determination of soil parameters are of vital importance for accurate soil modeling.

As mentioned above, only sand and clay will be studied in this thesis and this section will focus on material parameters for these two soil types.

2.3.1   Porosity

Because of the porous nature of soil, there are parameters that are used to determine the *porosity* of the soil. The porosity is denoted n and it is defined as

$$n = \frac{V_p}{V_t} \tag{2.1}$$

Here V_p is the volume of the pores and V_t is the total volume of the soil. According to [6], most soils has a porosity n of between 0.30 and 0.45.

Additionally, one can use the *void ratio e* instead to define the amount of pores and it is calculated as

$$e = \frac{V_p}{V_s} \tag{2.2}$$

Note here that V_s is the volume of the solids in the soil. The two measures can be related to each other since $V_t = V_s + V_p$. Conventionally, the void ratio e is preferred over the porosity n, cf. [9].

2.3.2   Saturation

As stated above, there may be water in the pores. However, air or some other gas may also be present and it is therefore useful to define a parameter S, which is the *degree of saturation* and it is defined as

$$S = \frac{V_w}{V_p} \tag{2.3}$$

V_w is the volume of the water in the soil and V_p is the volume of the pores, as above. The parameter indicates that $S = 1$ corresponds to a fully saturated soil whereas $S = 0$ represents a completely dry soil, as stated in [5].

2.3.3   Unit weight

Another important parameter is the *volumetric or unit weight γ* of a soil defined as

$$\gamma = \frac{W}{V_t} = \frac{mg}{V_t} = \rho g \tag{2.4}$$

where W is the weight of the soil, V_t is the volume of the soil, m is the mass of the soil, g is the acceleration of gravity and ρ is the density of the soil. The simplest possible way to obtain the unit weight γ is to measure the weight W and the volume V. However, if the weight and volume of the soil cannot be obtained by measurements or other means, the weight can be estimated with the help of the parameters introduced above as (cf. [6])

$$W = [Sn\rho_w g + (1-n)\rho_p g]\, V_t \tag{2.5}$$

Here ρ_w denotes the density of water and ρ_p is the density of the solid particles in the soil. The unit weight becomes

$$\gamma = \frac{W}{V_t} = Sn\rho_w g + (1-n)\rho_p g \tag{2.6}$$

If the porosity n, degree of saturation S and density ρ_p are known, the unit weight γ can thus be calculated. The unit weight defined in Equation 2.6 is often called the *moist unit weight*. If the soil is completely dry, i.e. $S = 0$, the unit weight is termed *dry unit weight* γ_d and is calculated as

$$\gamma_d = (1-n)\rho_p g \tag{2.7}$$

The opposite to dry unit weight, when $S = 1$, is the *saturated unit weight* γ_{sat}. Introducing the *specific gravity* $G_s = \rho_p/\rho_w$ and remembering that $\gamma_w = \rho_w g$, the saturated unit weight is obtained as

$$\gamma_{sat} = [G_s(1-n) + n]\,\gamma_w \tag{2.8}$$

However, the unit weight that is especially interesting in this thesis is the *submerged unit weight* γ', which is defined as

$$\gamma' = \gamma_{sat} - \gamma_w \tag{2.9}$$

The submerged unit weight γ' will be used in the finite element modeling in later chapters. It is the unit weight for all soil constituents excluding water in a completely saturated soil, according to [7].

2.3.4 Consolidation

The deformation of a soil is dependent on time as stated in the previous section. This could be due to creep, which is common for clay soils. However, another phenomenon that affects the deformation of a soil over time is called *consolidation*, cf. [6]. It is a process where the pore water is driven out from the soil, typically in compression when the pore space decreases. The rate of the water outflow depends on the *permeability* of the soil, where clay has a low permeability and sand a high permeability, as described in [10]. Therefore the consolidation process is longer for clay than for sand.

2.3.5 Drained and undrained analysis

Above it was explained that common practice is to divide the normal stresses $\boldsymbol{\sigma}$ into effective stresses $\boldsymbol{\sigma}'$ and *pore water pressure* $\boldsymbol{p}$, i.e. $\boldsymbol{\sigma} = \boldsymbol{\sigma}' + \boldsymbol{p}$. If the pore water pressure is known, the soil analysis is carried out in terms of effective stresses $\boldsymbol{\sigma}' = \boldsymbol{\sigma} - \boldsymbol{p}$, cf. [9]. Again, this separation of stresses only applies to normal stresses as shear stresses cannot be transferred by the pores, which also was stated above. If effective stresses are used in the soil analysis it is a *drained analysis* and an analysis with total stresses are called an *undrained analysis*. This is especially of importance when specifying the material parameters used in the constitutive model.

2.3.6 Mohr-Coulomb yield criterion

The Mohr-Coulomb criterion is widely used in geotechnical applications, cf. [11]. It is a criterion used to model the inelastic behavior of soils. The criterion assumes that the yield function is governed by the maximum shear stress (which is dependent on the normal stress) as

$$\tau_f = c + \sigma' \tan\varphi \tag{2.10}$$

Here τ_f is the maximum possible shear stress in an arbitrary plane, c is the *cohesion*, σ' is the normal effective stress and φ is the *angle of internal friction* or *friction angle*. In the criterion the effective normal stress σ' is used and in order to point out the use of effective or drained strength parameters, sometimes the cohesion and friction angle are written as c' and φ', respectively. The Mohr-Coulomb criterion and the involved parameters

can be illustrated by plotting Mohr's circle for states of stress in terms of maximum and minimum principal stress. Figure 2.1 shows the criterion for a drained analysis.
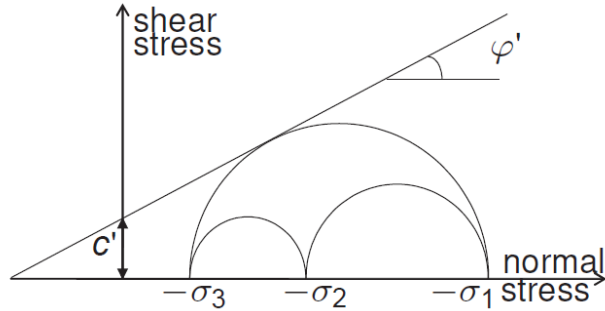

Figure 2.1: *Mohr-Coulomb criterion using drained strength parameters, adopted from [12]*

The straight line in the figure represents the yield line. The largest circle in the figure represents a state of stress at yielding and it precisely touches the yield line, meaning that additional loading will lead to yielding of the soil. A state of stress where the Mohr's circle is not in the proximity of the yield line is considered to be elastic. The Mohr-Coulomb criterion is an empirical criterion, cf. [5], and the strength parameters c' and φ' are not constants. They both depend on the initial state of the soil and the applied loading, leading to that they must be determined experimentally for accurate soil modeling, according to [10]. From the figure it can be concluded that c' is the intercept value on the shear stress axis and φ' is the slope of the yield line.

The pore water pressure is often unknown, therefore the engineer is forced to perform calculations with total stresses. According to [6], it is common in engineering practice to neglect the friction of the soil, i.e. assume $\varphi = 0°$. The analysis is simpler than an effective stress or drained analysis, and for a total stress or undrained analysis, the Mohr-Coulomb criterion takes the form as seen in Figure 2.2.
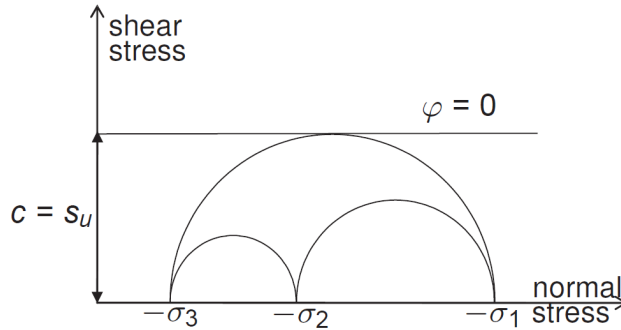
Figure 2.2: *Mohr-Coulomb criterion using undrained strength parameters, adopted from [12]*

In the figure it can be noted that the yield line is determined by the cohesion only, denoted by s_u. This is the *undrained shear strength* and the corresponding strain at this stress is denoted ϵ_{50}. The undrained shear strength is defined as (cf. [6])

$$s_u = \frac{1}{2}(\sigma_1 - \sigma_3) \tag{2.11}$$

It should be noted here that the principal stresses σ_1 and σ_3 are expressed in total stresses. When performing an undrained analysis, the Mohr-Coulomb criterion reduces to the well-known Tresca-criterion as $s_u = \tau_{max}$. However, this only applies to cohesive soils such as clay. In an undrained analysis of cohesion-less soils such as sand, the friction angle is non-zero together with a cohesion close to zero. For these soil types the Mohr-Coulomb yield line is largely determined by the (undrained) friction angle φ, as described in [5].

There are numerous constitutive models that describe the inelastic behavior of soils, with the Mohr-Coulomb criterion being the simplest to implement, as stated in [5]. For a more accurate analysis, more advanced constitutive models should be used but the Mohr-Coulomb criterion gives a good first approximation of the inelastic behavior. When modeling the soil as a continuum, the Mohr-Coulomb criterion is implemented in Abaqus/CAE and more information about this will be presented in Chapter 3.

2.3.7 Dilatancy

Dilatancy is a volume change that could occur when a soil is subjected to shear. An example of dilatancy for a dense sand is shown in Figure 2.3.

Figure 2.3: *Dilatancy for dense sand, from [6]*

In the figure, a dense sand is shown prior to loading (left). After applying a shear load the volume has expanded (right) since the sand particles are not as densely packed as before, ultimately making the sand looser. This is due to the fact that the particles shear over each other, cf. [6].

Dilatancy is measured with the *angle of dilation ψ*, which controls the amount of plastic volumetric strain developed during yielding. A value of $\psi = 0°$ corresponds to no volum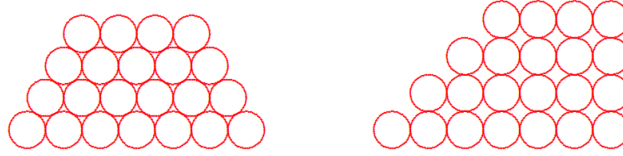e change, which is common for clay soils, as stated in [5]. For sand, the angle of dilation ψ is dependent on the friction angle φ and it can be estimated as $\psi = \varphi - 30°$. However, in most cases the assumption of $\psi = 0°$ can be adopted.

2.4 $P - y$ relationship

A $P - y$ relationship is used to model the interaction between a pile and the surrounding soil, denoted soil-pile interaction, where P is the lateral soil resistance and y is the lateral soil deflection. In practice, the relationship is used when designing laterally loaded piles, cf. [10]. The main idea is to calculate the ultimate soil resistance with analytical methods and relate this to the actual lateral soil resistance P. For more information about the analytical method the reader is referred to e.g. [13].

$P - y$ relationships are usually derived empirically and relate the lateral soil resistance P to the lateral soil deflection y. These non-linear $P - y$ curves describe the behavior of the soil when the pile is subjected to lateral loads, which is exactly the load case investigated in this thesis. More information about the load case is presented in Chapter 3.

2.4.1 Definition and history

The definition of P and y becomes clear with the help of Figure 2.4.
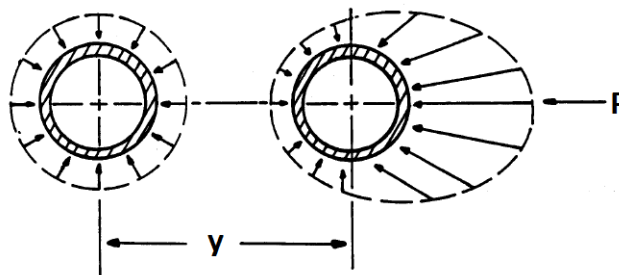
Figure 2.4: *Pile subjected to a lateral deflection y resulting in a lateral resistance P, modified from [13]*

In the figure a cylindrical pile has been subjected to a lateral deflection y. Before the deflection is applied, the unit stress distribution from the soil surrounding the pile is considered to be uniform and the stresses are normal to the pile's outer surface. When the pile has been deflected, Figure 2.4 shows that the stresses have decreased on the back side and increased on the front side of the pile. Integration of these unit stresses results in the lateral soil resistance P, acting in the opposite direction of the lateral deflection y. The dimensions of P and y are force per unit length and length, respectively.

The development of $P - y$ curves for piles was primarily carried out by Hudson Matlock (cf. [14]) and Lymon C. Reese (cf. [15] and [16]). Together they were involved in three major experimental programs in which a pile was subjected to short-term static loading and repeated (cyclic) loading, as stated in [13]. It should also be noted that the experiments were carried out in the presence of free water, i.e. the soil was submerged.

Matlock focused on soft clay and used a steel test pile with a diameter of 323.9 mm and a penetration in the soft clay of 12.80 meters. From his experiments, empirical formulas were developed to compute the lateral soil resistance P as a function of the lateral soil deflection y for soft clay, and for static and cyclic loading. The analytical relations were in line with the experimental results, as described in [14].

Reese's experiments involved stiff clay [15] and sand [16]. For stiff clay the steel test pile had a diameter of 609.6 mm and a penetration of 15.24 meters, whereas for sand the same pile was employed in the experiments but the penetration was 21.03 meters. For both experiments empirical formulas were developed and the correlation between the analytical and experimental results were good. The formulas for stiff clay and sand are however more complicated compared to the ones for soft clay, which will be shown below.

The empirical formulas developed from these three full-scaled experiments used to predict the lateral behavior of the soil have been widely accepted in geotechnical engineering, cf. [8]. They are implemented in several commercial softwares, such as ANSYS (cf. [17]) and LPILE (cf. [18]). However, numerous modifications to the $P - y$ relationship have been proposed, see for example [19], [20], [21] or [22], but the original relationship derived by Matlock and Reese will be considered in this thesis.

2.4.2 Method for constructing $P - y$ curves

The $P - y$ relationship is dependent on which type of soil that is studied and the material parameters of the soil. Additionally the type of loading and depth below the sea bed influence the $P - y$ curve as well, according to [2]. A soil's properties are dependent on the depth below the sea bed.

In this section the governing equations and the method used to produce $P - y$ curves are presented separately for soft clay, stiff clay and sand, all in line with [14], [15] and [16]. For computation of $P - y$ curves for soft and stiff clay subjected to cyclic loading, the reader is referred to Appendix A. As mentioned above, the field experiments were carried out on submerged soil, meaning that the method described below is only valid for soil in the presence of free water, i.e. soil below the water table.

Soft clay

For soft clay, we find the governing equations in [14]. The ultimate soil resistance P_u is given by the smallest value of the two equations

$$P_u = \left(3 + \frac{\gamma'}{s_u}X + \frac{J}{D}X\right)s_uD \tag{2.12}$$

$$P_u = 9s_uD \tag{2.13}$$

where

- P_u is the ultimate soil resistance [N/m]

- γ' is the submerged unit weight of soil [N/m^3]

- X is the depth below the sea bed [m]

- s_u is the undrained shear strength at depth X [Pa]

- D is the pile diameter [m]

- J is a dimensionless empirical constant, $0.25 \leq J \leq 0.5$, determined by field testing, common practice is to use 0.5 if no other information is available, cf. [14].

The ultimate soil resistance P_u is independent of the type of loading, otherwise the procedure to produce $P - y$ curves for soft clay is different for static and cyclic loading.

After computation of the ultimate soil resistance P_u, Equations 2.12 and 2.13 above, the deflection at one-half the ultimate soil resistance, y_{50}, is computed as:

$$y_{50} = 2.5\epsilon_{50}D \tag{2.14}$$

Here ϵ_{50} is the strain at one-half of the maximum principal stress difference, as stated above. With y_{50} known, the $P - y$ curve can be computed as:

$$P = \begin{cases} 0.5P_u \left(\frac{y}{y_{50}}\right)^{\frac{1}{3}} & 0 \leq y \leq 8y_{50} \\ P_u & y > 8y_{50} \end{cases} \tag{2.15}$$

A typical $P - y$ curve for soft clay subjected to static loading is shown in Figure 2.5.
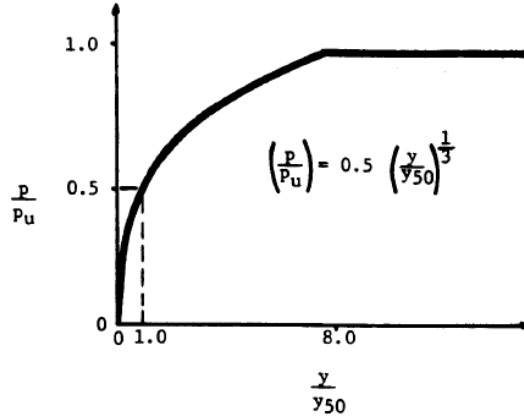
Figure 2.5: *Characteristic shape of a $P - y$ curve for soft clay (static loading), from [14]*

Stiff clay

The governing equations for stiff clay are found in [15]. For stiff clay it is recommended to use an averaged undrained shear strength s_a of the soil. The average should be computed over the depth X. Naturally, if the undrained shear strength is not varying over the depth, $s_a = s_u$. The ultimate soil resistance P_c is defined by the smallest value of the two equations

$$P_c = 2s_a D + \gamma' DX + 2.83 s_a X \tag{2.16}$$

$$P_c = 11 s_u D \tag{2.17}$$

where

- P_c is the ultimate soil resistance [N/m]

- s_a is the average undrained shear strength over the depth X [N/m^2]

After computation of the ultimate soil resistance P_c, the next step is to find a value of the constant A, where A_s corresponds to static loading and A_c corresponds cyclic loading, see Figure 2.6.

10
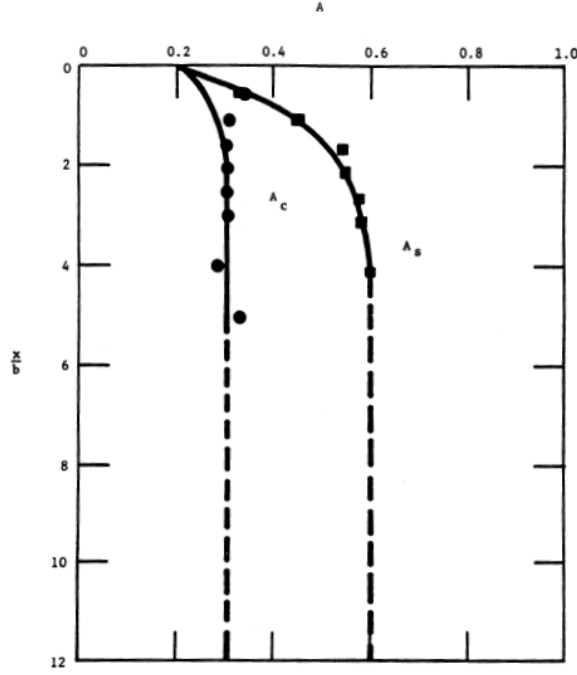
Figure 2.6: *Values of the constants A_s and A_c, from [15]*

In the figure it should be noted that on the vertical axis we have a characteristic non-dimensional depth $\frac{X}{D}$, where D is denoted by b in Figure 2.6. When A is known, the initial soil modulus k must be determined, which is a parameter used to define the initial elastic behavior of the soil. Just as for A, k is dependent on the type of loading but the average undrained shear strength s_a also has an influence. The initial soil modulus is found with the help of Table 2.2, which only should be used if no data is available.

Table 2.2: Initial soil modulus k for stiff clay, adopted from [15]

Average undrained shear strength s_a [kPa]	Initial soil modulus k [kPa/m]	
	Static	Cyclic
48-96	136000	54300
96-192	271000	108500
192-383	543000	217000

In the table above it should be noted that the initial soil modulus k for static loading is denoted k_s and for cyclic loading k_c. The last step that is equal for both static and cyclic loading is to compute y_{50} as

$$y_{50} = \epsilon_{50}D \tag{2.18}$$

For static loading, the $P-y$ curve for a stiff clay is calculated in a piecewise manner as

$$P = \begin{cases} k_s X y & y \leq y_{int} \\ 0.5P_c \left(\frac{y}{y_{50}}\right)^{0.5} & y_{int} < y \leq A_s y_{50} \\ 0.5P_c \left(\frac{y}{y_{50}}\right)^{0.5} - 0.055P_c \left(\frac{y-A_s y_{50}}{A_s y_{50}}\right)^{1.25} & A_s y_{50} < y \leq 6A_s y_{50} \\ 0.5P_c \left(6A_s\right)^{0.5} - 0.411P_c - \frac{0.0625}{y_{50}}P_c \left(y - 6A_s y_{50}\right) & 6A_s y_{50} < y \leq 18A_s y_{50} \\ 0.5P_c \left(6A_s\right)^{0.5} - 0.411P_c - 0.75P_c A_s & y > 18A_s y_{50} \end{cases} \tag{2.19}$$

In the equations defined in 2.19, y_{int} is the intersection point between the first two equations. If there is no intersection, i.e. y_{int} does not exist, the $P-y$ curve is calculated as

$$P = \begin{cases} k_s X y & \forall y \end{cases} \tag{2.20}$$

11

A typical $P - y$ curve for stiff clay subjected to static loading is displayed in Figure 2.7. Here it is assumed that the intersection point y_{int} exists.
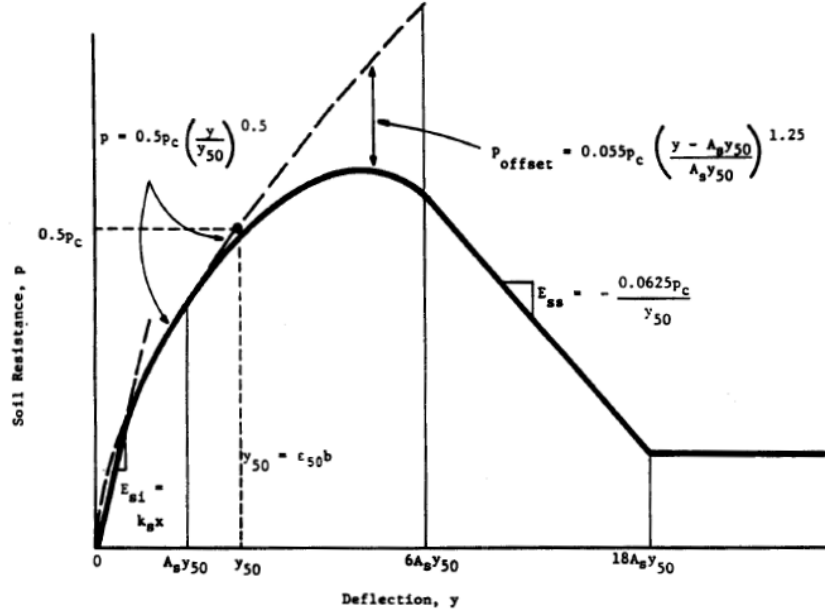
Figure 2.7: *Characteristic shape of a $P - y$ curve for stiff clay (static loading), from [15]*

Sand

The equations used to produce $P - y$ curves for sand are found in [16]. The first step is to make the preliminary computations based on the friction angle φ.

$$
\begin{aligned}
\alpha &= \frac{\varphi}{2} \\
\beta &= 45 + \frac{\varphi}{2} \\
K_o &= 0.4 \\
K_a &= \tan^2 \left(45 - \frac{\varphi}{2}\right)
\end{aligned}
\tag{2.21}
$$

After that, the ultimate soil resistance P_s is obtained by choosing the smallest value of the two equations

$$
P_s = \gamma' X \left[\frac{K_o X \tan \varphi \sin \beta}{\tan (\beta - \varphi) \cos \alpha} + \frac{\tan \beta}{\tan (\beta - \varphi)} \left(D + X \tan \beta \tan \alpha\right) + K_o X \tan \beta \left(\tan \varphi \sin \beta - \tan \alpha\right) - K_a D\right]
\tag{2.22}
$$

$$
P_s = K_a D \gamma' X \left(\tan^8 \beta - 1\right) + K_o D \gamma' X \tan \varphi \tan^4 \beta
\tag{2.23}
$$

where

- P_s is the ultimate soil resistance [N/m]
- φ is the friction angle [°]

When the ultimate soil resistance P_s is computed, two reference points, y_u and y_m, must be calculated. The first reference point is calculated as

$$
y_u = \frac{3D}{80}
\tag{2.24}
$$

For this point the lateral resistance is

$$
P_u = \overline{A} P_s
\tag{2.25}
$$

Here $\overline{A}$ is a constant determined by the non-dimensional depth $\frac{X}{D}$ and by the type of loading. For static loading the constant is denoted $\overline{A}_s$ and for cyclic loading the notation $\overline{A}_c$ is employed. The constant is determined with help of Figure 2.8.
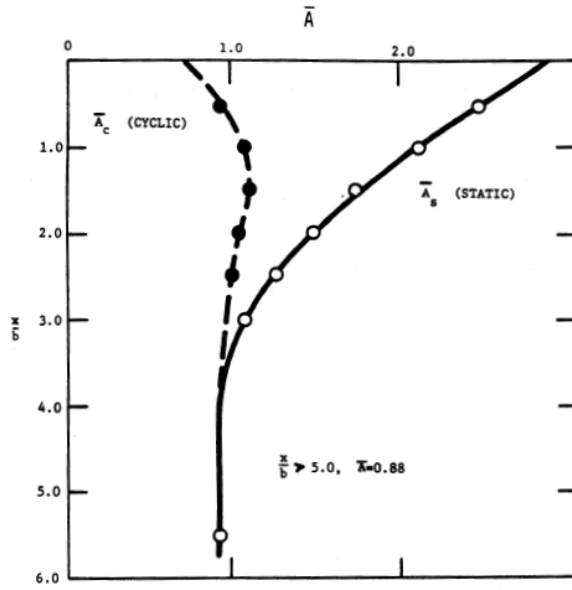
Figure 2.8: *Values of the constants $\overline{A}_s$ and $\overline{A}_c$, from [16]*

In the figure it should be noted that the pile diameter D is denoted by b. When the first reference point y_u is known, the second reference point y_m is calculated as

$$y_m = \frac{D}{60} \tag{2.26}$$

We introduce another constant B and for the second reference point the lateral resistance is

$$P_m = BP_s \tag{2.27}$$

Just as for the constant $\overline{A}$, B is determined by the non-dimensional depth and the loading type. B_s corresponds to static loading and B_c to cyclic loading. The value of the constant B is obtained from Figure 2.9.
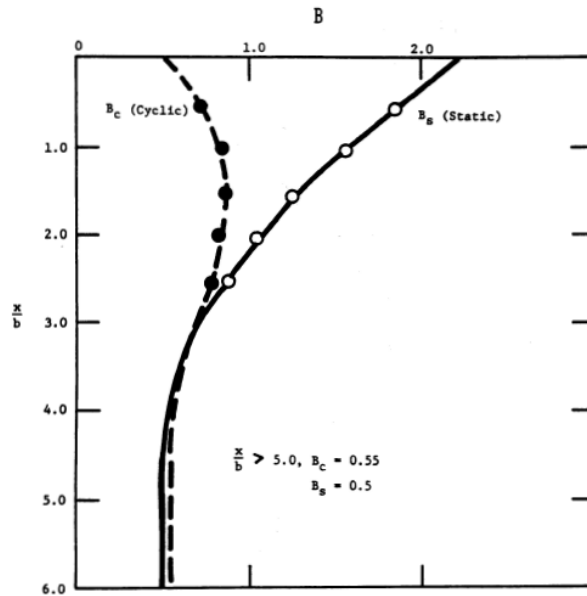
Figure 2.9: *Values of the constants B_s and B_c, from [16]*

13

Also in this figure b is equivalent to the pile diameter D. The final step before computing the $P - y$ curve is to establish the initial soil modulus k. It is a function of the relative density of the sand, which in turn is a function of the friction angle φ. If no data is available, an estimate of k is found in Table 2.3.

Table 2.3: Initial soil modulus k for sand, adopted from [16]

Friction angle φ [°]	Relative density	k [kPa/m]
< 30	Loose	5430
30 - 36	Medium dense	16300
> 36	Dense	33900

The procedure for computing $P - y$ curves for sand is the same for static and cyclic loading, where the loading type is incorporated in the constants $\overline{A}$ and B. The $P - y$ curve is constructed using

$$P = \begin{cases} kXy & y \leq y_k \\ \overline{C}y^{1/n} & y_k < y \leq y_m \\ m\,(y - y_m) + P_m & y_m < y \leq y_u \\ P_u & y > y_u \end{cases} \tag{2.28}$$

In the equation system above some new variables were introduced, namely the slope m, the power of the parabolic section n, the coefficient $\overline{C}$ and the intersection point y_k. They are calculated in the following way:

$$m = \frac{P_u - P_m}{y_u - y_m} \tag{2.29}$$

$$n = \frac{P_m}{m y_m} \tag{2.30}$$

$$\overline{C} = \frac{P_m}{y_m^{1/n}} \tag{2.31}$$

$$y_k = \left(\frac{\overline{C}}{kX}\right)^{\frac{n}{n-1}} \tag{2.32}$$

As mentioned above, y_k is an intersection point and defines the intersection between the first two equations displayed in 2.28. Just as for stiff clay, if there is no intersection, the first equation defines the whole $P - y$ curve, i.e.

$$P = \begin{cases} kXy & \forall y \end{cases} \tag{2.33}$$

Assuming that y_k exists, the typical shape of a $P - y$ curve for sand (at different depths X) is displayed in Figure 2.10.
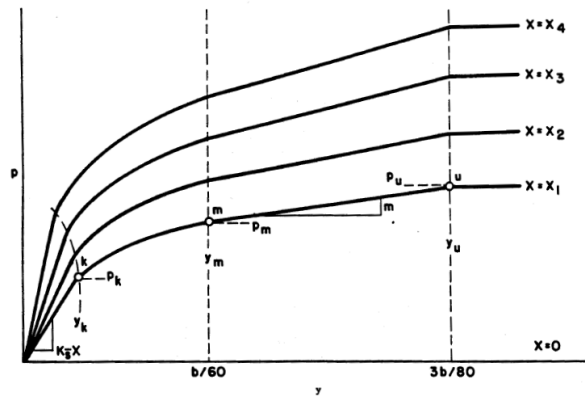
Figure 2.10: *Characteristic shape of $P - y$ curves for sand, from [16]*

14

2.4.3 Prediction of soil properties

To produce $P - y$ curves for a specific type of soil, certain properties of the soil must be known, as has been seen above. Some properties must be determined by tests but there exist guidelines in prediction of certain properties, such as the initial soil modulus k and the strain at one-half of the maximum principal stress difference ϵ_{50}. From tables introduced above, the reader finds some estimates of the initial soil modulus k. However, [14] and [15] present representative values of both k and the strain ϵ_{50} for different types of clay, where the average undrained shear strength s_a defines the clay type. These representative values could be used in the absence of more accurate data and they are shown in Table 2.4.

Table 2.4: Representative values of k and ϵ_{50}, adopted from [14] and [15]

Type of clay	s_a [kPa]	k_s [kPa/m]	k_c [kPa/m]	ϵ_{50}
Soft	12-24	8140	-	0.02
	24-48	27150	-	0.01
Stiff	48-96	136000	54300	0.007
	96-192	271000	108500	0.005
	192-383	543000	217000	0.004

For sand some representative values for the initial soil modulus k as a function of relative density were presented above (see Table 2.3). However, a more specific suggestion of how to predict k is given in [3] in the form of Figure 2.11 below.
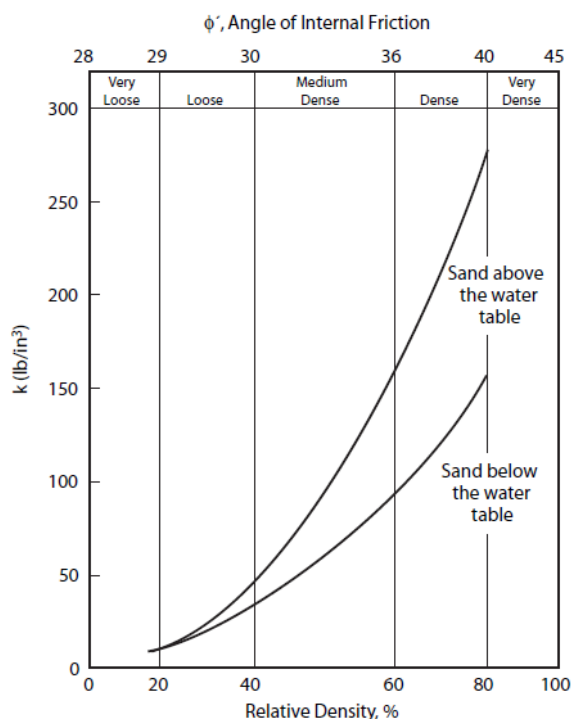
Figure 2.11: *Representative values of initial soil modulus k for sand, from [3]*

As stated above, only submerged soil (below the water table) is of interest and the lower graph in Figure 2.11 should be used when predicting the initial soil modulus k for sand. The following conversion factor is of use

$$1 \text{ lb/in}^3 = 271450 \text{ Pa/m} \tag{2.34}$$

For all other soil properties, sufficient tests should be carried out. For the interested reader, proposed tests are presented in [6] for both soft and stiff clay and for sand.

2.4.4   Comments and further reading

The $P - y$ relationship is considerably influenced by the soil data used. Extensive field testing of the actual soil studied should be carried out to obtain accurate soil data, and full-scale tests is the best possible way of defining a soil's properties, as stated in [3].

The approaches presented for clay and sand are general guidelines if no other information is available. Other methods to produce $P - y$ curves may be used if these are proven to be more accurate.

A phenomenon called scour, which is seabed sediment erosion due to wave and current action, can occur around offshore piles, cf. [23]. The lateral resistance of the soil could be lowered due to scour, and this should be taken into account during pile foundation design. For more information about scour and how to take the phenomenon into account in the analysis, the reader is referred to e.g. [24].

Finally, no information about layered soils have been presented. One could use the methods depicted above but it should be noted that the results could be non-conservative. An approach for developing $P - y$ curves for layered soils is outlined in [25]. The approach takes the overlying soil layers into account when predicting the lateral resistance P. In short, the procedure is based on finding the equivalent depth of all the layers existing below the upper-most layer. For example, to find the $P - y$ curve for the second layer one assumes that the first layer consists of the same soil type as the second layer, and what the equivalent depth of the first layer must be to obtain the same ultimate resistance P_u for the first and second layer at the interface. Then, to obtain the $P - y$ curve for the second layer, the equivalent depth is used instead of the actual depth.

The method to produce $P - y$ curves for submerged soft clay, stiff clay and sand has been implemented in MATLAB. To validate the MATLAB implementation, comparisons with the commercial software LPILE have been performed. There are many different material parameters involved in computation of $P - y$ curves and it is important that the implementation in MATLAB is correct as the lateral resistance P and deflection y will serve as input to modeling of the soil in Abaqus/CAE later on. The validation can be found in Appendix B.

2.4.5   Input to Abaqus/CAE

It should be noted that the lateral resistance P has units of force per meter. When implementing non-linear springs in Abaqus/CAE, a force-displacement behavior of the spring is needed as input. Therefore, the lateral resistance P is multiplied with the span range of the actual spring so it has the units of force, as is required in Abaqus/CAE. This is in accordance with [2].

3 Finite element modeling

This chapter describes the finite element model. As previously mentioned, Abaqus/CAE has been used to build the model. This chapter is divided into initial modeling, soil modeling with non-linear spring and continuum soil modeling.

3.1 Initial modeling

Before modeling the soil either with non-linear springs or as a continuum, the geometry and properties of the wellhead are presented. Also the load case is described and comparisons between a full model and a symmetric model will be presented.

3.1.1 Geometry and material model

As mentioned above, a simplified geometry of the wellhead assembly will be used in the simulations. In reality the wellhead assembly consists of several parts, such as surface casings, conductor housings and casings and several other details, cf. [2]. However, this thesis focuses on the soil-structure interaction and especially the modeling of the soil. Hence a simplified geometry of the wellhead assembly is used and only the wellhead itself is modeled. The wellhead is a cylindrical pipe of length 60 meters with outer diameter 36" (0.9144 m) and inner diameter 32" (0.8128 m), meaning a thickness of 2" (0.0508 m). In Abaqus/CAE such a pipe was created, both a full model and a symmetric model. The reason for using a symmetric model is obvious and it was validated against the full model, which is covered later in this section. The models created are shown in Figure 3.1.

(a) *Full model*　　　　　　　　　　(b) *Symmetric model*
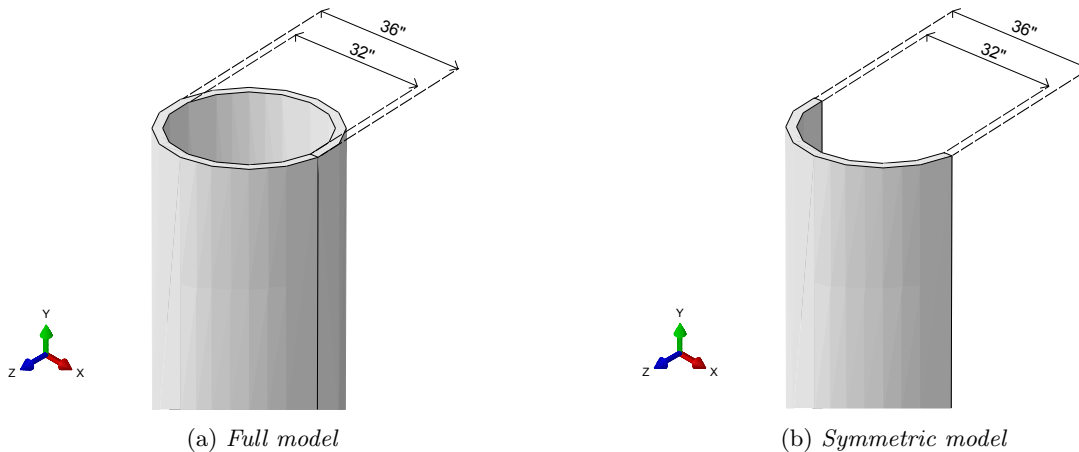
Figure 3.1: *The two models of the wellhead created in Abaqus/CAE*

In Figure 3.1 the coordinate system is also shown, and it will be referenced several times throughout this document. The material of the wellhead is steel with a Young's modulus of $E = 210$ GPa, a Poisson's ratio of $\nu = 0.3$ and a density of $\rho = 7850$ kg/m^3, as stated in [2]. A linear elastic material model is employed for the wellhead in Abaqus/CAE.

3.1.2 Boundary conditions

For the initial model where the soil is excluded, the lower boundary of the wellhead was constrained in all degrees of freedom for both the full and the symmetric model. Symmetric boundary conditions were applied at the cut boundary of the half model. The load is such that we have symmetry in the z-direction, meaning that for the symmetric model, the deformation in z-direction and the rotation about the x- and y-axes for degrees of freedom located at the cut boundary is constrained. The boundary conditions are displayed in Figure 3.2.

(a) *Symmetric boundary*   (b) *Lower boundary*
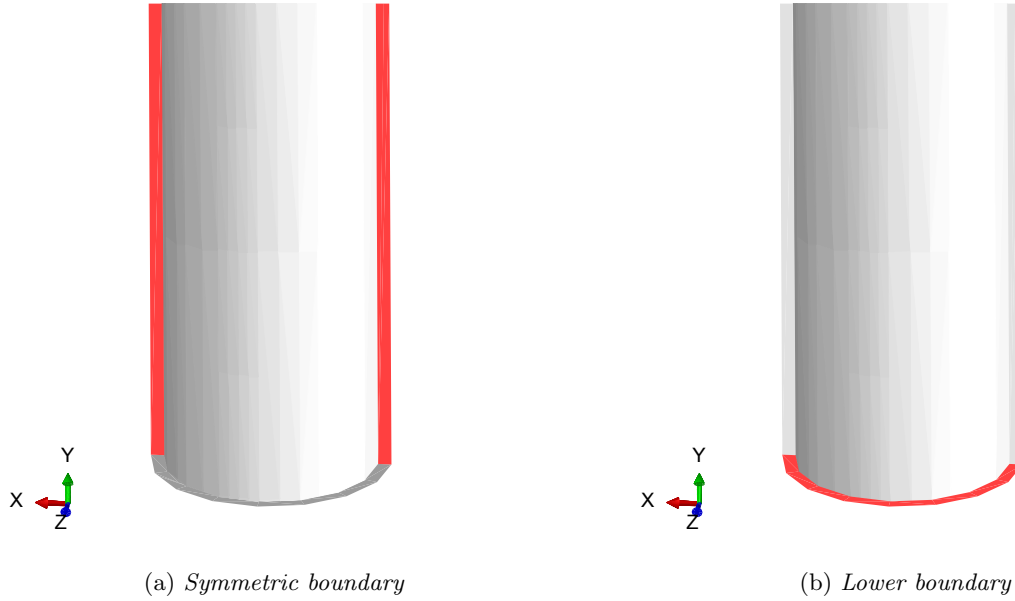
Figure 3.2: *Boundary conditions for the initial finite element model*

3.1.3 Loads

The wellhead is 60 meters long and the sea bed is located 3 meters below the top of the wellhead. Also, there are two critical points of interest on the wellhead, located 2.5 and 13 meters below the top, respectively. Circumferential butt welds are present in these points and therefore the stress in these areas are of particular interest. A rough estimation of the fatigue requirements on the wellhead is 500 days of operation with the rig. The load is assumed to be cyclic with a stress ratio of $R = -1$, i.e. an alternating load. The time it takes to complete one cycle is $T = 5$ s, leading to that the wellhead should be able to sustain $N_f = 8640000$ cycles before being replaced.

For the complete wellhead assembly a transverse load is applied in a region located approximately 10 meters above the top of the wellhead. Consequently a bending moment and a transverse load are assigned at the top of the wellhead in the finite element model in Abaqus/CAE. The magnitude of the transverse load is determined with the help of Euler-Bernoulli beam theory and the recommended practice for fatigue design of offshore steel structures found in [26]. This document presents $S - N$ curves in sea water for a detail similar to the wellhead with circumferential butt welds. With $N_f = 8640000$ cycles we obtain a stress range of $\Delta\sigma = 67.44$ MPa. With the assumed stress ratio of $R = -1$, the maximum stress allowed is $\sigma_{max} = 33.72$ MPa. Because of the transverse load, the bending stress or the stress in the y-direction σ_y will be dominant and it is assumed that the maximum stress allowed should be equal to the bending stress, i.e. $\sigma_{max} = \sigma_y$. Now, using classical Euler-Bernoulli beam theory the bending stress can be estimated as

$$\sigma_y = \frac{M_b z}{I} \tag{3.1}$$

where

- M_b is the bending moment

- z is the distance from the center axis

- I is the second moment of area of the wellhead's cross-section, $I = \frac{\pi}{64}\left(D_2^4 - D_1^4\right)$

- D_1 is the inner diameter of the wellhead

- D_2 is the outer diameter of the wellhead

The second critical point located 13 meters below the top of the wellhead would be the natural choice when dimensioning the transverse load against fatigue, as the bending moment would be larger in this point compared to the first critical point. However, when soil is introduced in the model, the second point of interest is affected

18

by the soil interaction, and the stress will be lowered. Therefore, the first critical point, located 2.5 meters below the top of the wellhead will be used when determining the magnitude of the transverse load with respect to fatigue, as it is not affected by the soil since the sea bed is located 3 meters below the wellhead top. For $z = \frac{D_2}{2}$, i.e. at the outer surface of the wellhead, and by applying the bending moment $M = 10T$, where T is the transverse load, it is easy to solve for the transverse load with respect to fatigue at the first critical point as

$$\sigma_y = \sigma_{max} = \frac{M_b z}{I} = \frac{12.5 T D_2}{2I} \Rightarrow T = \frac{\sigma_{max} 2I}{12.5 D_2} \approx 76.07 \text{ kN} \tag{3.2}$$

The applied bending moment at the top of the wellhead is thus $M = 10T = 760.7$ kNm. For the symmetric model the loads were multiplied with 0.5 to account for the symmetry. To implement the load case in Abaqus/CAE, a reference point was created on the symmetry axis at the top of the wellhead. The transverse load and bending moment were applied at the reference point and a coupling constraint between the reference point and the top surface was implemented. The transverse load T acts in positive x-direction and the bending moment M is a negative rotation about the z-axis. Figure 3.3 shows the applied loads at the top of the wellhead.
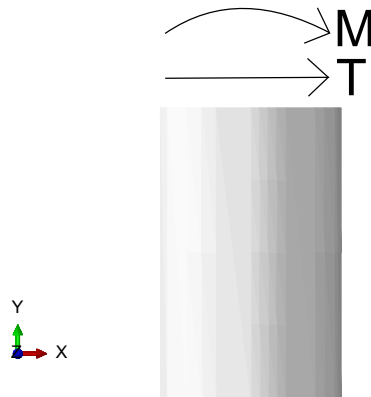
Figure 3.3: *Transverse load T and bending moment M*

In Abaqus/CAE, the user can choose either from a kinematic coupling constraint or a distributing coupling constraint. According to [27], the kinematic coupling constraint forces the coupling nodes to follow the rigid body motion of the reference point, whereas a distributing coupling constrains the motion of the coupling nodes to the translation and the rotation of the reference point, a so called node-force distribution. When employing a kinematic coupling constraint, the degrees of freedom for the coupling nodes are eliminated and there can be no relative motion between the nodes on the coupled surface, in this case the top surface of the wellhead. For the actual load case, the two coupling constraints will give similar results. If a twisting moment is applied at the reference point and warping of the structure would be expected, relative motion between the coupling nodes is required and the distributing coupling constraint must be used, which is described in [27]. In this investigation a distributed coupling was used for the loads. Preliminary analyses showed that there was in principle no differences between the kinematic and distributing coupling constraint.

3.1.4 Mesh

The wellhead was modeled with solid elements, entitled C3D20R in Abaqus/CAE, meaning brick elements with quadratic approximation with 20 nodes and reduced integration. A preliminary mesh for both the full and symmetric model were generated. DNV suggests in [2] that a minimum of 64 elements should be used in the circumferential direction for the full model, i.e. 32 elements for the symmetric model. 3 elements in the thickness direction was specified and the elements had a global size of approximately 0.1 meters.

3.1.5 Model comparison

The two models have been verified against the analytical value of the bending stress, and the symmetric model has also been verified against the full model to make sure the setup of the symmetric model is correct for further analyses. As a first step, the bending stress has been examined for three points on the outer surface of the wellhead and the results are shown in Table 3.1.

Table 3.1: Comparison between simulations results and analytical stress values

Distance from top [m]	Bending stress σ_y [MPa]		
	Full model	Symmetric model	Analytical value
2.5	33.75	33.75	33.72
13	62.10	62.10	62.04
50	162.00	162.00	161.85

The result from both the full and symmetric model are close to the analytical value and it is concluded that the initial finite element modeling is correct. Also, the results from the two finite element models are similar and the setup of the symmetric model seems to be accurate.

To obtain a lower computation time, linear elements, C3D8R and C3D8I, have been compared to the quadratic ones introduced above. Table 3.2 shows the results.

Table 3.2: Comparison between different element types for the two models

Distance from top [m]	Bending stress σ_y [MPa]					
	Full model			Symmetric model		
	C3D8R	C3D8I	C3D20R	C3D8R	C3D8I	C3D20R
2.5	33.16	33.84	33.75	33.16	33.84	33.75
13	61.02	62.27	62.10	61.02	62.27	62.10
50	159.18	162.43	162.00	159.18	162.43	162.00

The element types C3D8R and C3D8I are linear bricks with 8 nodes, with the first type using reduced integration and the second type utilizes something called incompatible modes, which improves the bending behavior by introducing internal deformation modes to the elements, as described in [27]. This prevents shear locking and correctly estimates the stiffness of the elements, leading to a more accurate stress prediction compared to regular linear element types, such as C3D8R. In Table 3.2 it can be observed that the stress results when using C3D8I- or C3D20R-elements are similar, and for the C3D8R-elements the stress is somewhat lower, with a difference of about 2 percent compared to the other element types. This is mainly because of the overestimation of the stiffness that occurs when using regular linear element types. For further analyses, the linear C3D8I-elements will be used instead of the quadratic C3D20R-elements to improve the computation time.

A mesh convergence study has also been carried out and increasing the number of elements in the thickness direction or lowering the global approximate size does not have an influence on the results, whereas when increasing the number of elements in the circumferential direction the bending stress converges towards the analytical value. However, the difference in stress between the analytical value and the simulation results above is less than a percent and the preliminary mesh described above is considered to be accurate enough. Additionally, the computation time significantly increases with increasing number of elements and keeping the initial mesh discretization gives a short computation time.

The last initial comparison without modeling the soil has to do with the placement of the reference point, in which the loading is applied. For the full model the point is naturally placed at the symmetry axis and in the analyses above the same placement has been used for the symmetric model. However, some differences in the stress results close to the top of the wellhead were observed for the two models, which lead to the need of further investigations. The distributing coupling constraint transfers the applied loads in the reference point to nodes at the top surface and the distance from the reference point to the nodes influences the magnitude of the nodal forces, according to [27]. Therefore, the placement of the reference point has a direct impact on the transferred nodal forces and subsequently the final results. To investigate the placing of the point, another symmetric model was created, henceforth called COG model, but with the reference point placed in the center of gravity in the xz-plane, which is easily found by the use of classical mechanical equations. The three models with their respective placement of the reference point are shown in Figure 3.4 below.

(a) *Full model*   (b) *Symmetric model*   (c) *COG model*
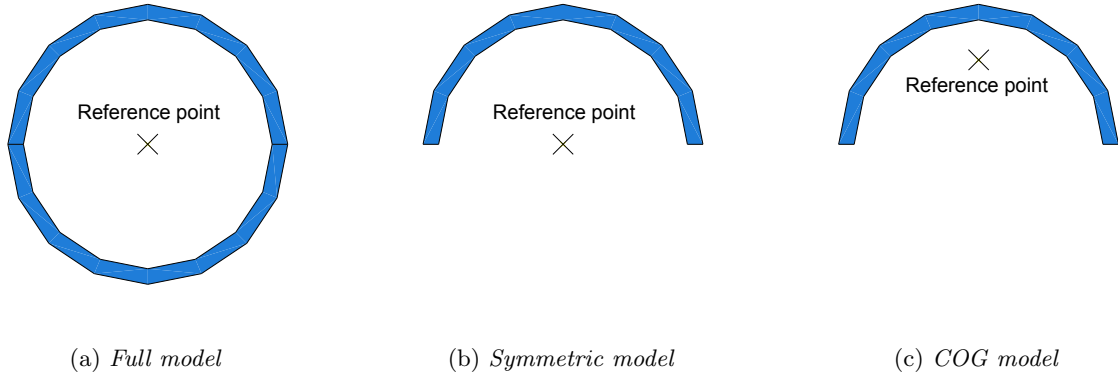
Figure 3.4: *Placement of reference point for the three models (view from above)*

The difference between the two symmetric models is clearly seen. Simulations have been carried out for all three models with the setup explained above. However, it should be noted that linear C3D8I-elements were used for all three models. The von Mises equivalent stress σ_e^{vM} at the outer surface of the wellhead was examined and the simulation results are shown in Table 3.3.

Table 3.3: Comparison between von Mises equivalent stress for the three models

Distance from top [m]	σ_e^{vM} [MPa]		
	Full model	Symmetric model	COG model
0	30.45	23.86	30.45
0.5	28.34	29.31	28.34
1.5	31.13	31.13	31.13
2.5	33.84	33.84	33.84
13	62.27	62.27	62.27
50	162.71	162.44	162.71

Comparing with the two tables above, the von Mises equivalent stress σ_e^{vM} is similar to the bending stress σ_y, which indeed confirms that the bending stress is the dominant stress for the wellhead. Concerning the results in Table 3.3, there is a rather large difference in stress just at the top of the wellhead between the full and symmetric model, about 20 percent, whereas the COG model gives a similar result compared with the full model. Further away from the top, the stresses obtained in the symmetric model converge towards the full model results and for large distances the full and symmetric model yield the same result. Worth noting is that the results from the COG model are similar to the full model for the whole wellhead and for further analyses, the COG model will be used. To further symbolize the difference between the three models, Figure 3.5 shows the von Mises equivalent stress on the outer surface of the wellhead for the first two meters below the top.
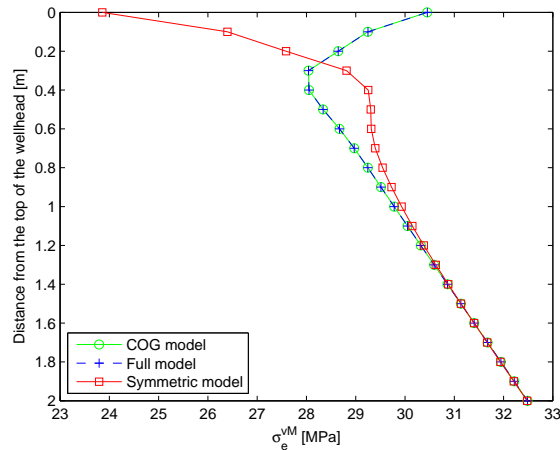
Figure 3.5: *von Mises equivalent stress close to the top of the wellhead for all three models*

In Figure 3.5 it is noted that close to the top of the wellhead the stress results from the symmetric model are noticeably different compared to the other two models. The full model and the COG model give in principle identical results.

The purpose of the model comparison in the initial finite element modeling was to validate the finite element model of the wellhead itself, to make sure that it is correct when introducing soil into the model. Initial simulations have proved that the modeling setup described above can be considered correct. However, when modeling the soil-structure interaction the boundary conditions and mesh of the wellhead can be altered if deemed necessary.

3.2 Soil modeling with non-linear springs

When modeling the soil with non-linear springs, the end points of the springs are attached to the structure and to the ground. Figure 3.6 shows the conventional setup of using lateral non-linear springs to represent the soil.
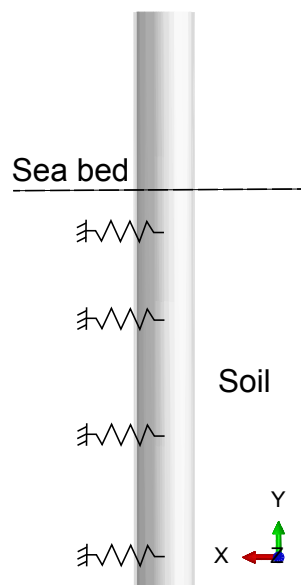
Figure 3.6: *Soil modeled with non-linear springs*

In the figure the x-direction is the lateral deflection of the springs. When introducing $P - y$ curves, the notation y was used for the lateral deflection to be consistent with existing literature. In this thesis when the soil is

22

modeled with non-linear springs the reader should be aware that the lateral deflection of the springs is in the x-direction of the finite element model.

In the previous section it was determined that the COG model of the wellhead should be used to obtain accurate results. The placement of the loading reference point was in the center of gravity in the xz-plane. When implementing non-linear springs in Abaqus/CAE, reference points must be used just as for the applied loading, and these were placed in the center of gravity, in line with the placement of the loading point.

When modeling the soil with non-linear springs, the short-term static response of the wellhead has been investigated. In reality the wellhead is subjected to cyclic loads but fatigue is not studied in this thesis, and the static response is considered. A particular result of interest is the lateral deformation at the top of the wellhead, as this result notably affects the fatigue analysis of the complete wellhead assembly, cf. [2].

3.2.1 Implementation of non-linear springs

As a first step the way to implement non-linear springs in Abaqus/CAE was investigated. There are many options available and a correct configuration must be used in order for the non-linear springs (and subsequently the soil) to behave properly. In Abaqus/CAE there exists an option called *Springs/Dashpots* which, at first glance, fits the purpose. However, using this option the user is restricted to linear springs, and connectors are a valid alternative to model non-linear spring behavior. When creating a connector, which can be either linear or non-linear, the user must first create a wire between two connecting points. In our case the first connecting point is the spring reference point and the second connecting point is the ground, as stated in [2]. A connector's behavior can be specified by force-displacement or moment-rotation data. The non-linear springs representing the soil are one-dimensional and the lateral, i.e. in x-direction, force and displacement, need to be specified. The *Connection Type* was set to *Cartesian* in order to be able to use the global coordinate system for the connectors, as described in [27].

The connectors or the non-linear springs, must be attached to the structure, i.e. the wellhead. This can be done in several ways but according to [2] the soil springs should be connected to all of the exterior nodes of the wellhead solid elements facing the soil. In this thesis the soil springs have been attached to the wellhead in two ways, via outer edges or via outer surfaces, together with distributing coupling constraints and reference points. Regardless of the attachment type, the span range of the spring is the same. The two attachment types are displayed in Figure 3.7.
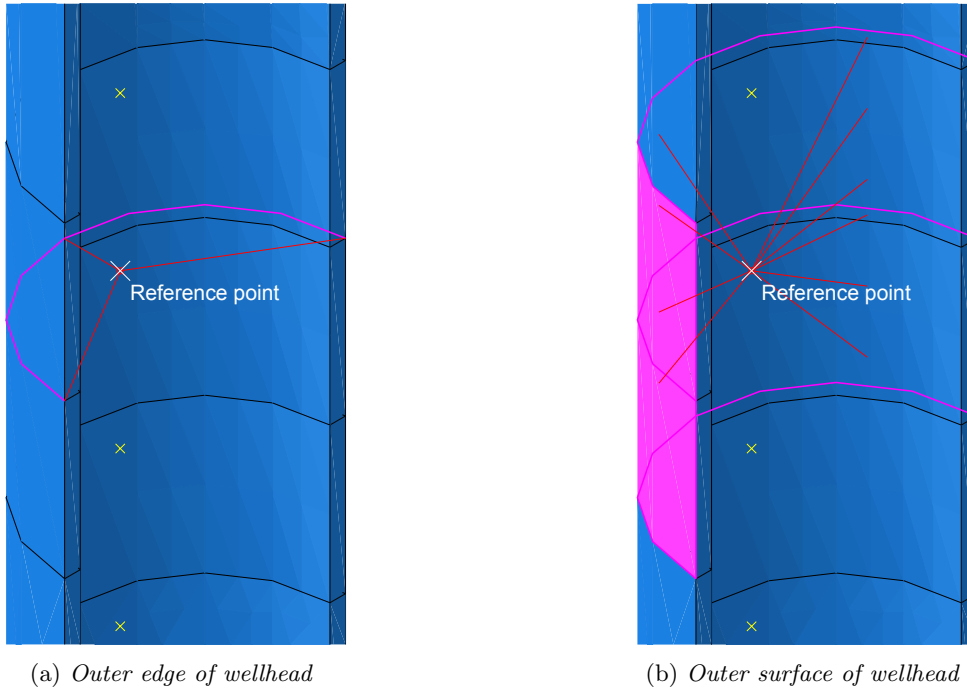

(a) *Outer edge of wellhead*   (b) *Outer surface of wellhead*

Figure 3.7: *The two attachment types considered*

To verify the connector setup, linear connectors with varying constant stiffness k were created at different

depths, i.e. the connectors represented linear springs. Simulations were carried out and the forces in the connectors were noted. For a linear spring the spring force can be calculated analytically as $F = kx$, where x is the displacement. The connector forces matched analytical values for both attachments to the structure, which indicates that the connector setup is correct.

When specifying non-linear springs using connectors, the force-displacement behavior is obtained from $P - y$ curves in the way presented in Section 2.4. For each connector, the force and displacement are specified in the form of tabular values, which are obtained from the computed spring forces and deflections in MATLAB. Initial simulations were carried out with some non-linear connectors included in the finite element model, and the results showed that Abaqus interpolates between tabular values to find the connector force for a specific deflection and that eventual extrapolation is constant, just as it should be. Worth noting is that all spring forces should be multiplied with 0.5 when using symmetric models, cf. [2].

Implementing non-linear springs in Abaqus/CAE could be repetitive and time-consuming, especially if a large number of springs is included in the finite element model. Therefore it is useful to create a script, preferably in Python, to minimize the implementation time. The script should be able to implement the soil springs in Abaqus/CAE based on given positions and span ranges. Because of the advantages of using a general script, one has been created in Python and it is divided into the following steps:

- Read spring positions and span ranges

- Create reference points at specified positions

- Connect the reference points to the wellhead via a distributing constraint, using both outer edges and outer surfaces as the attachment type

- Create one wire for each reference point, connected to the point and the ground

- Create connectors with force-displacement behavior from an already generated file from MATLAB

- Assign each connector to its respective wire

In order to use the script, the user needs to specify the position and span range for each spring. Also, force-displacement behavior data for each spring must have been generated in MATLAB prior to execution of the script. Nonetheless, the script is extremely useful for creating different spring discretizations in an effective way.

3.2.2 Reference solution

To be able to evaluate different soil springs discretizations, a reference solution must be computed. The reference solution is considered to be the exact solution and all other configurations will be compared with it. As the sea bed is located 3 meters below the top of the wellhead, there are 57 meters of soil that needs to be modeled. Preliminary analyses showed that modeling one spring every meter of soil were sufficient to capture the soil's behavior in a realistic way and higher spring densities did not affect the results. Thus, in the reference configuration, 57 springs is modeled at the following depths below the sea bed: 0.5 m, 1.5 m, 2.5 m etc. This is a largely exaggerated number of springs and a lower number of springs should be sufficient to obtain accurate results, as will be seen below.

3.2.3 Case study

When modeling the soil with non-linear springs, three different soil compositions were investigated. The first two compositions were homogeneous soils with constant (with depth) properties, whereas the third consisted of a layered soil. Before introducing the properties for the three examined cases, the finite element modeling setup for the wellhead is shown. In the initial finite element modeling section some conclusions regarding the setup were drawn and it is therefore good to have an updated overview of the wellhead modeling setup. The following applies to the wellhead when the soil is modeled with non-linear springs:

- COG model used in all analyses with a linear elastic material model with $E = 210$ GPa and $\nu = 0.3$

- A mesh with 32 elements in the circumferential direction, 3 elements in the thickness direction and a global size of 0.1 meters with C3D8I as the element type

24

- The lower boundary of the wellhead constrained in the axial direction (y-direction), together with one node constrained in the x- and z-direction to prevent rigid body motion

- Symmetric boundary condition (symmetry in z-direction) applied at the cut boundary, meaning no deformation in the z-direction and no rotation about the x- and y-axes

- The loads (transverse load and bending moment) applied at the top surface via a reference point and a distributing coupling constraint with transverse load $T = 38.035$ kN and bending moment $M = 380.35$ kNm, see Figure 3.3

The wellhead setup is similar to that explained above and the main change is the boundary condition at the lower boundary, see Figure 3.2. It was changed to better reflect the behavior of the wellhead in the soil and thus obtain a more realistic finite element model. The change will however have little effect on the results, as the wellhead is 60 meters long. As for the placement of the springs, DNV suggests in [2] several depths below the sea bed to place springs to model the soil in a realistic way, but mentions nothing about different types of soil. Therefore, the purpose of the case studies is to find the optimal spring discretization needed to accurately model the soil, and if the discretization varies for different soil compositions. The spring discretization proposed by DNV will not be investigated here, as the focus lies on understanding how to implement non-linear springs to model the soil.

Looking back at the soil properties, all soils are assumed to be completely saturated, i.e. $S = 1$, meaning that all pores in the soil are completely filled with water. The submerged unit weight γ' is thus calculated using Equations 2.8 and 2.9 as

$$\gamma' = \gamma_{sat} - \gamma_w = ([G_s(1-n)+n]-1)\gamma_w \tag{3.3}$$

In order to calculate the submerged unit weight the porosity n and the specific gravity G_s of the soil are needed. In Section 2.3 the porosity of soil were presented to be $0.30 \leq n \leq 0.45$. Typical values of specific gravity for different soil types are given in [10]. For sand a typical value is $G_s = 2.67$ and for clay $G_s = 2.70$. Regarding the undrained shear strength s_u and the corresponding strain at this stress ϵ_{50} for clay, these parameters are found with the help of Table 2.4. The friction angle φ which is used when computing $P - y$ curves for sand is taken from [10], where typical values are listed.

CASE A

The first soil composition consists of a homogeneous stiff clay and the following properties were used:

- $n = 0.3$

- $G_s = 2.70$

- $\gamma' = ([G_s(1-n)+n]-1)\gamma_w = 11.67$ kN/m^3

- $s_u = 150$ kPa

- $\epsilon_{50} = 0.005$

As the soil is homogeneous, the average undrained shear strength s_a and the undrained shear strength s_u is equal and the initial soil modulus is $k = 271000$ kN/m^3, see Table 2.4. The $P - y$ curves have been computed for stiff clay subjected to static loading, see Equation 2.19. Because of the constant outer diameter of the wellhead D, the only parameter that is not constant when computing the $P - y$ curves is the depth X.

Reference solution

The von Mises equivalent stress of the wellhead and deformation in the x-direction have been examined. Figure 3.8 shows the results for the entire wellhead along an edge where $x = D/2$ and $z = 0$, meaning the outer surface of the wellhead.

(a) *von Mises equivalent stress*
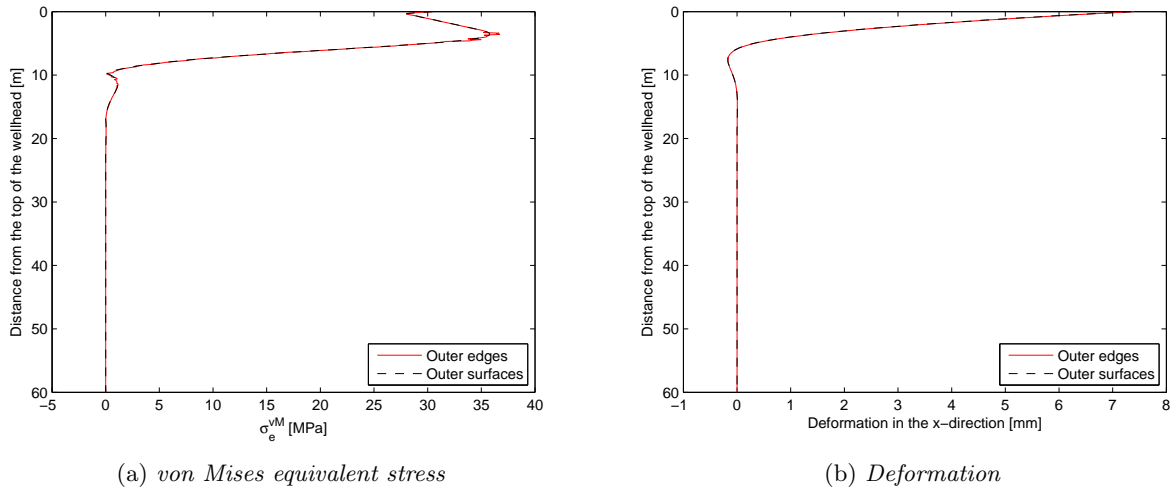
(b) *Deformation*

Figure 3.8: *Results from the reference configuration for case A*

At about 20 meters below the top of the wellhead the stress and deformation are zero due to the stiff clay. This means that the spring density far away from the wellhead top does not have a large influence on the results. For further configurations, the number of springs should be lowered in this region. Another thing worth noting is that for the outer edges coupling type, there are some peaks in the stress. These peaks occur exactly where a spring is located, due to the springs being attached to just an edge instead of a whole surface. It is therefore preferred to attach the springs to surfaces instead of edges, thus obtaining a smoother stress curve, which is seen in Figure 3.8a. However, for the deformation the two coupling types give the same results, cf. Figure 3.8b. The sea bed is located 3 meters below the top of the wellhead, and for these first meters the soil will have no influence on the results. This is clearly seen by the linear stress response close to the top of the wellhead, cf. Figure 3.8a.

Additional configurations

With a reference solution computed the number of springs can now be varied and iteratively a configuration can be found that agrees with the reference results above. In the additional configurations, the number of springs is high in the region where the stress and deformation are non-zero and low in the region with zero stress and deformation, cf. Figure 3.8. Three additional configurations were created and they are shown in Table 3.4, where it should be noted that range and depth refers to the sea bed.

Table 3.4: Additional configurations for case A

Spring number	Configuration 2 Range [m]	Configuration 2 Depth [m]	Configuration 3 Range [m]	Configuration 3 Depth [m]	Configuration 4 Range [m]	Configuration 4 Depth [m]
1	0 - 1	0.5	0 - 1	0.5	0 - 1	0.5
2	1 - 3	2	1 - 2	1.5	1 - 2	1.5
3	3 - 5	4	2 - 3	2.5	2 - 3	2.5
4	5 - 10	7.5	3 - 5	4	3 - 4	3.5
5	10 - 15	12.5	5 - 7	6	4 - 5	4.5
6	15 - 20	17.5	7 - 10	8.5	5 - 7	6
7	20 - 25	22.5	10 - 14	12	7 - 9	8
8	25 - 35	30	14 - 20	17	9 - 12	10.5
9	35 - 45	40	20 - 27	23.5	12 - 15	13.5
10	45 - 55	50	27 - 37	32	15 - 19	17
11	55 - 57	56	37 - 47	42	19 - 24	21.5
12			47 - 57	52	24 - 34	29
13					34 - 44	39
14					44 - 54	49
15					54 - 57	55.5

26

As a first step configuration 2 was created and evaluated against the reference configuration. This resulted in configuration 3 as the results from configuration 2 were in good agreement with the ones displayed in Figure 3.8, but there were some substantial differences close to the sea bed. Therefore, as seen in Table 3.4, the spring density for configuration 3 near the sea bed is somewhat higher compared to configuration 2. The third configuration proved to be more accurate than the second, but an additional fourth configuration were needed to successfully match the results from the reference configuration.

The main difference between the three additional configurations is the spring density near the sea bed, indicating that the soil discretization in this region has a direct influence on the results. At the lower half of the wellhead, the spring density is similar for all three configurations meaning that a low number of springs in this region is acceptable for accurate results.

A particular result of interest is the deformation in the x-direction at the top of the wellhead. This is used as input for the complete fatigue analysis of the wellhead assembly, which was mentioned above. The deformation at the top of the wellhead for the three additional configurations have been compared with the one obtained in the reference configuration and Table 3.5 shows the results for both coupling types. The deformation for the reference configuration was 7.345 mm and 7.397 mm for the outer surfaces and outer edges coupling type, respectively.

Table 3.5: Deformation difference at the top of the wellhead for case A

	Configuration 2		Configuration 3		Configuration 4	
	Surfaces	Edges	Surfaces	Edges	Surfaces	Edges
Difference [%]	1.45	3.51	0.23	0.31	0.042	0.044

In Table 3.5, it can be noted that for the deformation at the top, the result from all three additional configurations are in good agreement with the result from the reference configuration. The reason for creating three additional configurations were that configuration 2 and 3 did not match the reference configuration results for the whole wellhead, whereas the results from the optimal discretization in the fourth configuration are in principle identical to the results seen in Figure 3.8. The number of springs have decreased from 57 in the reference configuration to 15 in the optimal configuration. Looking at Table 3.5 again, it is of interest that the outer surfaces coupling type proves yet again that it is preferred over the outer edges coupling type, as for a given spring discretization the difference is higher for the latter coupling type.

CASE B

The second case studied was a homogeneous soft clay with the following constant properties employed:

- $n = 0.4$

- $G_s = 2.70$

- $\gamma' = 10.01$ kN/m^3

- $s_u = 30$ kPa

- $\epsilon_{50} = 0.01$

The $P - y$ curves have been computed for soft clay subjected to static loading, cf. Equation 2.15, with $J = 0.5$.

Reference solution

Just as for case A, the von Mises equivalent stress and deformation in the x-direction have been investigated. Figure 3.9 shows the stress and deformation results for the wellhead along an edge where $x = D/2$ and $z = 0$.

(a) *von Mises equivalent stress*

(b) *Deformation*

Figure 3.9: *Results from the reference configuration for case B*

For soft clay, the stress and deformation are zero at about 35 meters below the top of the wellhead. Because of the soft clay, the spring density must be high in a larger region compared to the stiff clay in case A. In further configurations the number of springs will be lowered where the stress and deformation are zero. Looking at the stress in Figure 3.9a, there are some peaks in the stress for the outer edges coupling type, however they are not as apparent as in case A. Just as in case A, the deformation for case B is similar for the two coupling types, see Figure 3.9b. Worth noting is that the deformation close to the top of the wellhead is significantly higher in case B compared to case A. This is expected because of the soft clay soil.

Additional configurations

Exactly as in case A, an optimal configuration can be found iteratively. The spring density should be high where the stress and deformation are substantial and low in the zero region. Because of the soft clay, more springs are needed in case B than in case A. As stated above, the non-zero region for soft clay are larger compared to the stiff clay in case A which indicates that a higher number of springs in additional configurations for case B are needed to obtain results in good agreement with the reference configuration results. Two additional configuration were created and the spring discretizations are shown in Table 3.6.

Table 3.6: Additional configurations for case B

Spring number	Configuration 2		Configuration 3	
	Range [m]	Depth [m]	Range [m]	Depth [m]
1	0 - 1	0.5	0 - 1	0.5
2	1 - 2	1.5	1 - 2	1.5
3	2 - 4	3	2 - 3	2.5
4	4 - 6	5	3 - 5	4
5	6 - 8	7	5 - 7	6
6	8 - 10	9	7 - 9	8
7	10 - 13	11.5	9 - 11	10
8	13 - 18	15	11 - 13	12
9	18 - 24	21	13 - 15	14
10	24 - 30	27	15 - 18	16.5
11	30 - 37	33.5	18 - 21	19.5
12	37 - 47	42	21 - 24	22.5
13	47 - 57	52	24 - 30	27
14			30 - 37	33.5
15			37 - 47	42
16			47 - 57	52

Just as in case A, configuration 2 was created as a first step and evaluated against the results from the reference configuration. An improved configuration was then created, namely configuration 3, and it was considered accurate enough compared with the reference configuration. Just as for case A, the spring density for the additional configurations in case B at the lower half of the wellhead are similar and the difference between the two lies in the spring density at the upper half of the wellhead.

Also here the deformation at the top of the wellhead have been investigated and the results are shown in Table 3.7. The deformation for the reference configuration was 21.478 mm and 21.519 mm for the outer surfaces and outer edges coupling type, respectively.

Table 3.7: Deformation difference at the top of the wellhead for case B

	Configuration 2		Configuration 3	
	Surfaces	Edges	Surfaces	Edges
Difference [%]	0.50	0.55	0.13	0.19

From Table 3.7 it is clearly seen that the second configuration is sufficient to accurately predict the deformation at the top of the wellhead. The third configuration is however more accurate, but with a difference of about 0.5% for both coupling types in configuration 2, it can be considered to be a precise discretization. Looking at the stress and deformation for the whole wellhead, the difference between configuration 2 and 3 were more substantial with the third configuration coming out on top, with the number of springs decreased from 57 in the reference configuration to 16 in the optimal discretization or configuration.

As opposed to case A, the difference between the two coupling types are not so large and for soft clay the outer edges coupling type is a viable choice. This was indicated in the stress curve, see Figure 3.9a, where the peaks in the stress were not that prominent as for the stiff clay in case A, cf. Figure 3.8a. Lastly, the deformation at the top of the wellhead is relatively large in case B when comparing to case A, which is expected for the soft clay.

CASE C

The third soil studied is a layered soil as mentioned above. The layered soil is composed of different types of clay and sand, as shown in Figure 3.10.
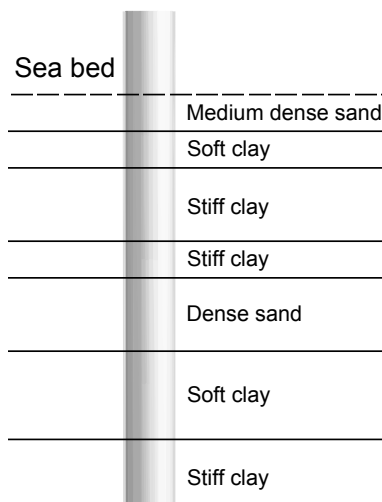

Figure 3.10: *Layered soil studied in case C*

In total there are seven layers and the respective properties for each layer is shown in Table 3.8. For all clays the specific gravity was assumed to be $G_s = 2.70$ and for sand a value of $G_s = 2.67$ was used.

Table 3.8: Properties for the layered soil studied in case C

Depth below sea bed [m]	Soil description	n	γ' [kN/m³]	s_u [kPa]	ϵ_{50}	φ [°]
0-5	Medium dense sand	0.45	9.01	-	-	33
5-10	Soft clay	0.4	10.01	20	0.02	-
10-20	Stiff clay	0.35	10.84	80	0.007	-
20-25	Stiff clay	0.32	11.34	100	0.005	-
25-35	Dense sand	0.42	9.50	-	-	38
35-47	Soft clay	0.37	10.51	45	0.01	-
47-57	Stiff clay	0.3	11.67	200	0.004	-

The properties for the different soil layers in the table are completely fictitious and are only meant to represent the soil types in a realistic way. Moving on, it is assumed that within each soil layer, the properties are constant, e.g. $s_u = s_a$ in a layer. The $P - y$ curves for the different layers have been computed for static loading according to Section 2.4. The layered soil approach described in Section 2.4.4 is not implemented in MATLAB and therefore it was intentional that the studied layered soil consisted of one sand layer at the top and one at a deep depth below the sea bed. This is because the layered soil approach has a rather large influence on the $P - y$ curve for sand at low depths, cf. [28]. With the soil composition in Table 3.8 the layered soil approach should thus have little influence on the $P - y$ curves and the curves computed in MATLAB can be considered accurate.

Reference solution

Figure 3.11 shows the von Mises equivalent stress and deformation results for the wellhead along the same edge studied in case A and B.
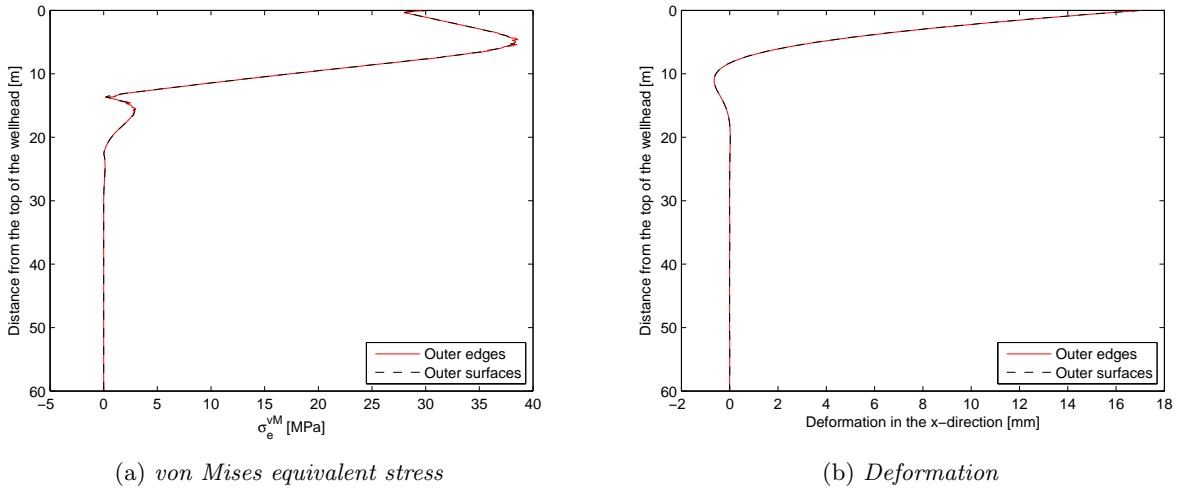

(a) *von Mises equivalent stress* (b) *Deformation*

Figure 3.11: *Results from the reference configuration for case C*

For a layered soil it is hard to predict the behavior of the wellhead because of the inhomogeneous soil composition. Nonetheless, because of the soil in case C consisting mostly of clay the shape of the stress and deformation curve should be similar to the results from case A and B, which Figure 3.11 clearly shows. Also, the first two layers below the sea bed consists of sand and soft clay, indicating that the deformation should be larger than for the stiff clay in case A, which is seen in Figure 3.11b. Moving on, the stress and deformation tends to zero at about 30 meters, thus leading to the need of a high spring density for the upper half of the wellhead and a low number of springs for the lower half. Just as for case B, the peaks in the stress for the outer edges coupling type in case C (Figure 3.11a) are not as apparent as in case A. As expected, the two coupling types give the same deformation of the wellhead, cf. Figure 3.11b.

Additional configurations

When modeling a layered soil with $P - y$ curves, an engineer is not as free to do what he wants in terms of spring discretization compared with a homogeneous soil. This has to do with the soil being split up into different layers, each with its own properties. A soil spring cannot cover more than one layer at a time meaning that the engineer is forced to take this constraint into consideration when modeling the soil springs. Depending on the soil composition, this could lead to a large number of springs even if that is not required. Anyhow, for case C where the non-zero region is about the upper half of the wellhead, two additional configurations were evaluated and they are displayed in Table 3.9.

Table 3.9: Additional configurations for case C

Spring number	Configuration 2		Configuration 3	
	Range [m]	Depth [m]	Range [m]	Depth [m]
1	0 - 1	0.5	0 - 1	0.5
2	1 - 2	1.5	1 - 2	1.5
3	2 - 3	2.5	2 - 3	2.5
4	3 - 5	4	3 - 4	3.5
5	5 - 7	6	4 - 5	4.5
6	7 - 10	8.5	5 - 6	5.5
7	10 - 13	11.5	6 - 8	7
8	13 - 16	14.5	8 - 10	9
9	16 - 20	18	10 - 12	11
10	20 - 25	22.5	12 - 14	13
11	25 - 30	27.5	14 - 17	15.5
12	30 - 35	32.5	17 - 20	18.5
13	35 - 41	38	20 - 25	22.5
14	41 - 47	44	25 - 30	27.5
15	47 - 57	52	30 - 35	32.5
16			35 - 41	38
17			41 - 47	44
18			47 - 57	52

Just as for case B, only two additional configurations were needed in case C to match the results from the reference configuration. Both the second and third configuration have a rather large number of springs compared to the other two cases. This is a direct consequence of studying a layered soil. However, for both additional configurations the spring density is equally low at the lower half of the wellhead, and for the upper half of the wellhead configuration 3 has a slightly higher number of springs than the second configuration.

The difference in the deformation at the top of the wellhead compared to the reference configuration is shown in Table 3.10. The deformation for the reference configuration was 17.008 mm and 17.052 mm for the outer surfaces and outer edges coupling type, respectively.

Table 3.10: Deformation difference at the top of the wellhead for case C

	Configuration 2		Configuration 3	
	Surfaces	Edges	Surfaces	Edges
Difference [%]	1.08	1.46	0.025	0.016

In case C, the two configurations are in good agreement with the deformation result at the top of the wellhead from the reference configuration, with a difference of a little more than 1% for both coupling types for the second configuration. The discretization in the second configuration was however not sufficient compared to the reference results overall and therefore configuration 3 was created, which is in good agreement with the reference configuration and predicts the deformation at the top of the wellhead accurately, which is seen in Table 3.10. The number of springs in the optimal discretization for the layered soil is 18, which means a decrease in springs with about 70% compared to the reference configuration.

For the layered soil in case C, the outer edges coupling type is a feasible choice when connecting the springs to the wellhead, just as in case B. The difference between the two coupling types is not large and the outer

edges coupling type actually predicts the deformation at the top more accurately for the optimal configuration, as seen in Table 3.10.

3.2.4 Final comments

With the Python script described above, it is easy to model the soil with non-linear springs and switch between different configurations and finally obtain an optimal configuration. To use non-linear springs is a simple approach to model the soil and the computation time is short because of the one-dimensional soil springs. Because of this, $P - y$ curves and non-linear springs are frequently used in geotechnical engineering, as stated in [8].

If the attention is turned towards the case study above, it is clear that the optimal discretization is highly dependent on the soil composition. It is of course dependent on the load case as well where high loads would require more springs to truly capture the soil's behavior. For all case studies however, the applied load have been the same and the difference between the three cases lies in the soil composition. For the stiff clay in case A, the deformation is relatively low, leading to that a small number of springs is required to predict an accurate wellhead response. In case B, the soft clay required a larger number of springs compared to the stiff clay, which was expected because a low stiffness leads to larger deformations. The only difference between the two soil compositions in case A and B is the stiffness, which has a big impact on the deformation of the wellhead, and subsequently the number of springs required to obtain an accurate model of the soil.

Moving on to the layered soil in case C, the magnitude of the deformation is in between the two first cases. This is expected as the layered soil consists of mostly soft and stiff clay layers, and two sand layers. The optimal discretization in case C is actually constructed with the highest number of springs of all cases, and this has to do with the individual soil layers and their unique properties, as explained above. When studying a layered soil, one spring cannot be modeled over two different layers.

For all three cases an optimal discretization or configuration matching the reference solution have been found. These optimal configurations are dependent on the soil composition as discussed above, but also on the loading. For the applied load case (transverse load and bending moment at the top of the wellhead) these configurations will model the soil and predict the response of the wellhead in an accurate way. If the magnitude of the loads would have been lower, fewer springs would have been needed to obtain an accurate response and vice versa for higher loads.

One could argue that the springs should be placed in accordance with the reference configuration to be on the safe side in terms of soil modeling. For this simple model, the difference in computation time between the reference configuration and the additional configurations is negligible. For the fatigue analysis of the complete wellhead assembly however, the number of springs impacts the computation time significantly and it is desirable to find an optimal discretization with as few springs as possible.

A final note on the optimal discretization is that the recommended placement of springs suggested by DNV in [2] mentions nothing about the type of soil. The results above clearly show that the soil composition has a big influence on the spring placement and if using the discretization presented by DNV regardless of the composition of the soil, one could end up with an inaccurate model. It is therefore recommended to investigate the placement of springs in terms of wellhead response and iteratively find a suitable discretization.

In all three cases studied there is a zero stress occurrence some distance from the top of the wellhead, with a slight increase followed by a decrease to zero again, see e.g. Figure 3.8a. This phenomenon is explained by the cross-section bending moment induced in the wellhead. If no soil would have been modeled the cross-section bending moment would naturally be a negative rotation about the z-axis for the whole wellhead because of the applied loads at the top. However, the soil introduced in the model induces a positive cross-section bending moment in the wellhead and when the stress tends to zero, the cross-section bending moments induced by the applied loads and by the soil perfectly balance each other, explaining the absence of stress. The followed slight increase in stress occurs because the cross-section bending moment turns positive in a small region and later tends to zero for large depths. Figure 3.12 shows the induced cross-section bending moment in the wellhead just before and immediately after the first zero stress occurrence.
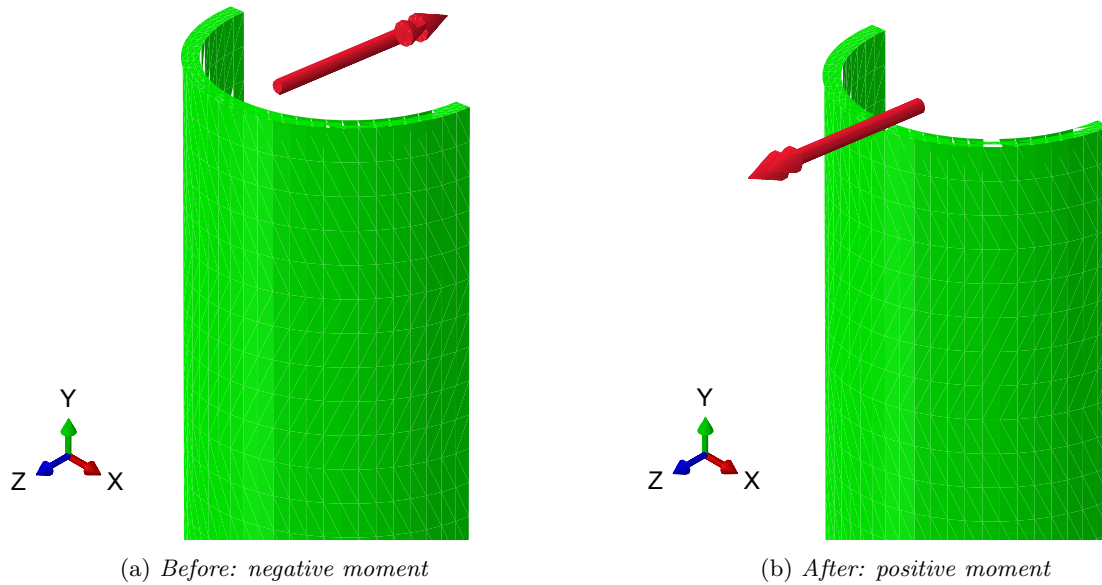
(a) *Before: negative moment*   (b) *After: positive moment*

Figure 3.12: *Cross-section bending moment close to the first zero stress occurrence*

In the figure the cross-section bending moment clearly changes sign, which also explains the negative deformation in the x-direction for the wellhead that occurs in a small region for all three cases, see e.g. Figure 3.8b. A negative cross-section bending moment leads to positive deformation and vice versa for a positive cross-section bending moment.

As all results above have shown, the outer surfaces coupling type is preferable when studying the stress of the wellhead. If the springs are connected to the outer edges of the wellhead, peaks in the stress where a spring is located occur. This is due to the fact that when connecting the springs to an outer edge, stress singularities arise and the stress results at, and close to, these outer edge connections are higher than what they should be. To eliminate these peaks in the stress, more springs could be implemented when modeling the soil. However, to preserve a low computation time, it is advantageous to use the outer surfaces coupling type and thus less springs are needed in the model. For the deformation of the wellhead, both coupling types are a viable choice when connecting the springs to the structure as the results are similar, which was seen in the case study above.

One problem with the outer surfaces coupling type could be the amount of coupling degrees of freedom, or nodes, introduced in the model. For each coupling, a possible upper limit of number of degrees of freedom could be exceeded when introducing a coupling with a large span range. This is of course software-dependent, but Abaqus has such an upper limit. The outer edges coupling type does not suffer from this restriction, as the coupling is applied on an edge instead of a surface, regardless of the span range. This is especially important to take into consideration when implementing springs and couplings on the lower half of the wellhead. As these springs have little or no influence on the results (seen above), one want to create couplings with a large span range in this region as there is no need for a high spring density. This could violate the condition of maximum number of allowed coupling degrees of freedom when connecting the springs to the outer surfaces.

One approach to prevent the condition from being violated could be to model the wellhead with simpler elements instead of solid elements. As the results show above, both the deformation and the stress are zero at the lower half of the wellhead and there is no need to implement springs at these depths. To use beam elements with a certain stiffness at large depths suggested by DNV (cf. [2]) would be a feasible alternative to non-linear springs and $P - y$ curves. DNV suggests that the stiffness of the beam elements should be constant and this is in agreement with the $P - y$ curves, as the depth dependence vanishes for large depths, cf. Section 2.4.

3.3   Continuum soil modeling

After the initial finite element modeling and modeling the soil with non-linear springs, the next step is to model the soil as a continuum with solid elements. When modeling the soil as a continuum there are many factors to take into account for the soil, such as:

- Material model

- Geometry

- Mesh

- Contact properties between wellhead and soil

- Boundary conditions

- Loads

The most important factor is the material model, especially the constitutive model for the inelastic behavior. As mentioned before, the mechanical properties of a soil are often strongly non-linear and assuming a linear elastic response is usually not enough to accurately model the soil. Therefore, the importance of a pertinent constitutive model for the inelastic behavior cannot be stressed enough.

A parametric study will be carried out to understand how the different factors listed above contribute to the wellhead response. In Section 3.2, three different soil compositions were presented. For the continuum soil modeling, these three cases will be investigated as well to be able to compare the response for the two modeling strategies later on. A particular result of interest is the deformation in x-direction at the top of the wellhead. When modeling the soil with solid elements, an unconsolidated and undrained analysis will be carried out, cf. Section 2.3. Also, just as in Section 3.2, all soils are assumed to be completely saturated.

3.3.1 Material model

Prior to the parametric study, the alternatives to model the elastic and plastic behavior of the soil in Abaqus/CAE are investigated. According to [5], it is common for a continuum soil to employ a linear elastic material model in conjunction with a constitutive model for the plastic behavior. It should be noted that Hooke's isotropic law might not be appropriate for soils as they are often show anisotropic elastic behavior, as stated in Chapter 2. Nevertheless, soils are often idealized as being linear elastic and isotropic, especially when estimating foundation settlements, cf. [10].

When employing a linear elastic material model one can specify Young's modulus E_s and Poisson's ratio ν for the soil, but it would work just as well with shear modulus G and bulk modulus K as all four elastic moduli are related to each other. In Abaqus/CAE however, the user has to specify E_s and ν to successfully define the soil's elastic stiffness. As mentioned in the previous chapter, laboratory tests should be carried out to define a soil's properties. However, in the absence of available data, [10] presents typical value ranges of E_s and ν for different types of soil. One should be careful though, as actual field values depend on the stress history, water content, density and age of the soil. The recommended ranges of E_s and ν for clay and sand are given in Table 3.11.

Table 3.11: Range of E_s and ν, modified from [10]

(a) E_s

Soil type	Characteristics	E_s [MPa]
Clay	Very soft	2-15
	Soft	5-25
	Medium	15-50
	Stiff	50-100
Sand	Loose	10-25
	Dense	50-81

(b) ν

Soil type	Characteristics	ν
Clay	Saturated	0.4-0.5
	Unsaturated	0.1-0.3
Sand	Loose	0.2-0.35
	Dense	0.3-0.4

As no data is available for E_s or ν, representative values from Table 3.11 will be used when modeling the soil as a continuum.

Moving on to the inelastic behavior of the model, there are a lot of suitable constitutive models in Abaqus/CAE, namely Cam clay plasticity, modified and extended Drucker-Prager plasticity and Mohr-Coulomb plasticity. As mentioned in Chapter 2, the Mohr-Coulomb plasticity model or yield criterion is the simplest one to implement and therefore it will be used in this thesis. For information about the other plasticity models in Abaqus/CAE, the reader is referred to [27].

The Mohr-Coulomb criterion was described in detail in Section 2.3.6 and here the Abaqus/CAE implementation of the criterion will be discussed. In [27] it is stated that the criterion can be used to simulate the material response under monotonic loading, which is exactly the load case studied in this thesis. Furthermore, the criterion must be applied in conjunction with a linear elastic material model and isotropic hardening or softening can be modeled. It is also possible to specify a so called "tension cutoff", which limits the load carrying capacity in the tensile region. Nonetheless, the following parameters are needed in Abaqus/CAE to employ Mohr-Coulomb plasticity:

- Friction angle φ

- Dilation angle ψ

- Cohesion c

- Absolute plastic strain ϵ^p

In Section 2.3.6 it was stated that for an undrained analysis the friction angle $\varphi = 0°$ for clay whereas sand has a non-zero friction angle. The friction angles used for sand in the previous section with non-linear springs were found from representative values for saturated soils in [10]. The recommended friction angle in an undrained analysis for clay and sand is shown in Table 3.12.

Table 3.12: Representative values of φ for clay and sand, modified from [10]

Soil type	Characteristics	φ [°]
Clay	Saturated	0
Sand	Loose, saturated	28-34
	Dense, saturated	33-45

For the friction angle, the main difference between continuum soil modeling and $P - y$ curves is the use of φ for clay, which is not needed when computing the behavior of the non-linear springs, cf. Section 2.4.2.

Moving on to the dilation angle, it was described in Section 2.3.7 where it was stated that $\psi = 0°$ for clay and $\psi = \varphi - 30°$ for sand. This is a parameter not used when computing $P - y$ curves and it is interesting to see how a non-zero dilation angle influences the results.

In an undrained analysis the cohesion c is equal to the undrained shear strength s_u for clay and for sand the cohesion is close to zero, cf. Section 2.3.6. For an undrained analysis of sand, a cohesion $c = 1$ kPa is commonly assumed in engineering practice, see [12]. When computing $P - y$ curves for sand, the cohesion is not used (see Section 2.4.2) in contrary to continuum soil modeling where the cohesion is included to predict the inelastic behavior.

The last important parameter, is the absolute plastic strain ϵ^p. In Abaqus/CAE it can be used together with the cohesion to specify hardening or softening of the soil. For the continuum soil modeling it is assumed that the behavior of the soil is elastic-perfectly plastic meaning no hardening or softening. Comparing to $P - y$ curves for a static load case this is a reasonable assumption for soft clay and sand, see Figure 2.5 and Figure 2.10, respectively. For these two soil types the lateral resistance P increases gradually with the lateral deflection y and after a certain value of y, P is constant. For stiff clay, the assumption of a perfectly plastic behavior might be inaccurate, see Figure 2.7. In the figure it is seen that the lateral resistance P increases with the lateral deflection y up to a certain value, and increasing the deflection further leads to a lowering of P, until it becomes constant at large deflections. This softening of the stiff clay for a static load case is not considered in the continuum soil modeling and will be taken into account when comparing the results from the two methods to model the soil. The best alternative would be to perform laboratory tests on the actual soil studied and characterize the hardening or softening behavior, but in this thesis perfectly plastic behavior is assumed as no other data is available.

There are other parameters that could be specified in the Mohr-Coulomb plasticity model. These are associated with the flow rules incorporated in the criterion and no information about these will be given here. Instead the interested reader is referred to [27]. Also, the "tension cutoff" option will not be used.

To summarize, the material model of the soil consists of a linear elastic model and a Mohr-Coulomb constitutive model for the inelastic behavior. Assuming elastic-perfectly plastic behavior, five parameters are needed to implement the material model properly, namely:

- Young's modulus E_s

- Poisson's ratio ν

- Friction angle φ

- Dilation angle ψ

- Cohesion c

3.3.2 Geometry and mesh

The geometry of the soil is of vital importance to obtain realistic results. The extent of the soil is infinite and the geometry must be such that the soil boundaries do not influence the wellhead response. When creating the geometry of the soil it is advantageous to use a circular geometry in Abaqus/CAE. This allows the use of solid bricks combined with an accurate mesh algorithm, cf. [27].

Regarding the size of the circular soil geometry, there are some guidelines found in e.g. [29] and [30]. The latter paper suggests a radius of 11 times the pile or wellhead diameter and a vertical length of 1.7 times the length of the wellhead. One has to keep in mind that these dimensions are dependent on the load case and the type of soil studied. Therefore the effect of soil dimensions on the wellhead response will be investigated for each of the three cases studied.

As the wellhead utilizes the symmetry of the applied loads, this carries over to the geometry of the soil. It will be modeled as a solid half-cylinder with a certain radius and length, but with a space for the wellhead to fit into. Figure 3.13 shows the principal geometry of the soil created in Abaqus/CAE.
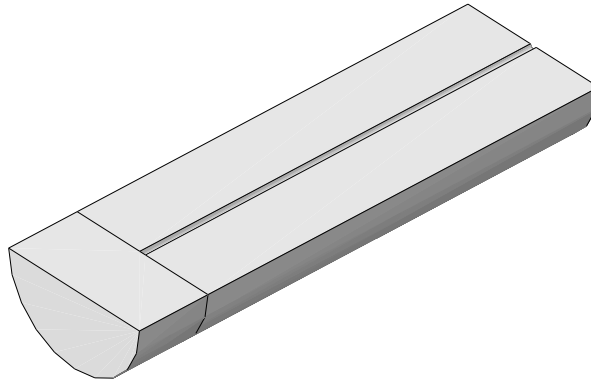

Figure 3.13: *Soil modeled as a solid half-cylinder with empty space for the wellhead*

In the figure above the radius of the soil is 11 times the outer diameter of the wellhead and the length is 70 meters. Note also the space for the wellhead with a vertical length of 57 meters, since the sea bed is located 3 meters below the top of the wellhead.

Moving on to the mesh for the soil, linear C3D8I-elements will be used, just as for the wellhead. Regarding the mesh size, one would expect that a small mesh size is required close to the wellhead and a larger mesh size far away from the most stressed region can be specified. Also, the mesh size can be quite large at large depths below the sea bed as the stress and deformation for the wellhead will be low in this region, as was seen when the soil was modeled with non-linear springs in Section 3.2.

In Abaqus/CAE there are linear infinite elements that can be used to simulate the infinite extent of the soil, see [27]. One element of interest is CIN3D8, a three-dimensional linear brick with 8 nodes. When using infinite elements the region modeled with finite elements is called near-field region and the far-field region consists of infinite elements. However, one has to be careful when using infinite elements, as the size of the infinite elements must be considerably larger than the finite elements in the mesh. The nature of infinite elements is such that the displacement tends to zero at the boundary of the far-field region and therefore the size of infinite elements must be large enough for this to be imposed. Figure 3.14 shows the wellhead mounted in the soil together with a near-field and far-field region.
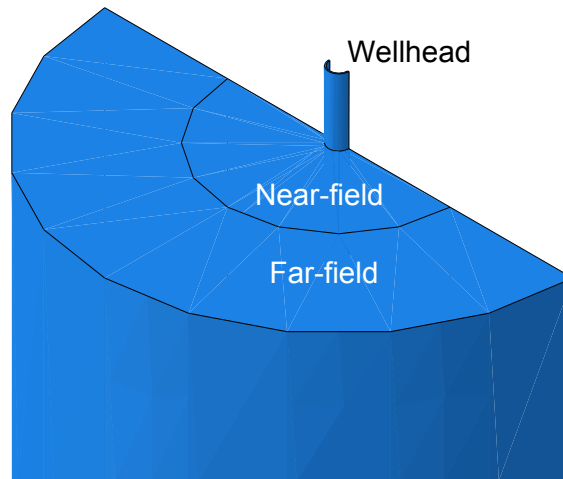
Figure 3.14: *Definition of near-field and far-field region*

Infinite elements are not available in the pre-processor Abaqus/CAE, hence the input file has to be manually edited to include these infinite elements in the model. A simple trick one can do in Abaqus/CAE is to select the regions where infinite elements should be and model these areas with three-dimensional acoustic elements with 8 nodes, termed AC3D8. After writing the input file the user can manually edit it and replace AC3D8 with CIN3D8. The reason for using AC3D8-elements is that the node definitions between the finite and infinite elements are correctly defined automatically.

The advantage of using a combination with finite and infinite elements instead of only finite elements is that the geometry of the soil could be smaller whilst still preventing the soil boundaries to affect the wellhead response. Another benefit is that infinite element boundaries serve as the boundary conditions, and no external boundary conditions need to be specified, as stated in [27]. The boundary condition for an infinite element is that the displacement will decrease linearly within the element, to zero just at the infinite boundary. The usage of infinite elements will be investigated for the three studied cases later in this section.

3.3.3 Contact properties

There are two contact areas for the soil and the wellhead, namely the circumferential boundary of the wellhead in contact with the surrounding soil and the lower boundary of the wellhead in contact with the soil below the wellhead. The most important contact is the circumferential one, where the normal and tangential behavior must be specified in Abaqus/CAE.

For the normal behavior it was decided to use a "hard" contact together with the penalty constraint enforcement method, cf. [27]. The default settings for the contact stiffness were used, meaning a linear relationship with a contact stiffness 10 times higher than a representative underlying element stiffness. Also, the surfaces in contact were allowed to separate.

Regarding the tangential behavior, also here the penalty algorithm was chosen as the constraint enforcement method. Abaqus/CAE requires a coefficient of friction between the surfaces in contact but this is unknown. The directionality of the friction was assumed to be isotropic and a value of $\mu = 0.5$ was used. All other settings for the tangential behavior were set to default. The influence of the coefficient of friction will be investigated later in this section.

The second contact involves the lower boundary of the wellhead and the underlying soil. This contact is modeled using a tie constraint, meaning that the two surfaces will undergo the same deformation. This constraint is considered accurate as in reality there are components below the wellhead connected to the reservoir, cf. Figure 1.1.

For both contact pairs surface-to-surface discretization was used with the wellhead as the master surface and the soil as the slave surface.

3.3.4 Boundary conditions

Moving on to the boundary conditions, they are dependent on what element types that are used in the mesh. If finite elements C3D8I are used for the whole soil, the circumferential and lower boundary of the soil are constrained in all degrees of freedom. This is due to the fact that far away from the wellhead, the soil should not undergo any deformation. On the other hand, if infinite elements are used in the far-field region, these serve as boundary conditions, as was discussed above. The influence of boundary conditions, or rather the element type used, will be investigated for the three cases. A correct implementation of finite elements in the near-field region and infinite elements in the far-field region will lead to a shorter computation time, as the near-field region can be smaller with a correct usage of infinite elements, according to [27].

3.3.5 Loads

The loads on the wellhead are the same as before, i.e. a transverse load and a bending moment applied at the top, see Figure 3.3. To get an estimation of the soil settlement, a gravity load is included for the soil. This settlement is interesting as the wellhead is mounted in the soil after it has settled. The gravity load is specified with an acceleration of $g = 9.81$ m/s^2 in the negative y-direction and a density for the soil. Looking back at Equation 2.4 in Section 2, the submerged density of the soil can be calculated as

$$\rho' = \frac{\gamma'}{g} \tag{3.4}$$

For the three cases studied, the submerged unit weight γ' is known and subsequently the submerged density ρ' for the soil can be evaluated. No gravity load for the wellhead is included in the static analysis as the focus is on how to model the soil as a continuum and what the wellhead response is because of the applied loads at the top.

The applied loads are thus the gravity load for the soil and the transverse load and bending moment from before. In Abaqus/CAE, the applied loads are divided into two steps where the first step introduces the gravity load for the soil and predicts the soil settlement. In the second step the loads at the top of the wellhead are introduced, while still maintaining the initial settlement of the soil due to gravity.

3.3.6 Initial finite element model

The finite element model of the soil has been described in words in the sections above, and for easier reference an overview of the initial modeling setup for the static short-term analysis is needed. The initial setup serves as the basis for the parametric study and the following applies to the wellhead and soil prior to the parametric study:

- Material model

    - **Wellhead:** Linear elastic material model with $E = 210$ GPa and $\nu = 0.3$
    - **Soil:** Linear elastic model in combination with a constitutive model of Mohr-Coulomb type (assuming perfectly plastic behavior) with E_s, ν, φ, ψ and c dependent on soil composition

- Geometry and mesh

    - **Wellhead:** COG model used in all analyses with a mesh consisting of 32 elements in the circumferential direction, 3 elements in the thickness direction and an approximate global size of 0.1 meters, together with C3D8I as the element type
    - **Soil:** Modeled as a solid half-cylinder (see Figure 3.13) with a certain radius and length with a mesh consisting of 15 elements in the circumferential direction and a global approximate size of 0.5 meters, together with C3D8I-elements or a combination of C3D8I- and CIN3D8-elements

- Contact properties

    - Mechanical contact between the circumferential boundary of the wellhead and the surrounding soil with normal behavior specified as a "hard" contact with the penalty constraint enforcement method and allowed separation after contact. The tangential behavior of the contact also utilizes the penalty algorithm with a coefficient of friction of $\mu = 0.5$

    – A tie constraint modeling the contact between the lower boundary of the wellhead and the underlying soil

- Boundary conditions and loads

    – Symmetric boundary conditions (symmetry in z-direction) applied on the corresponding boundaries of the wellhead and the soil, meaning no deformation in the z-direction and no rotation about the x- and y-axes

    – Circumferential and lower boundaries of the soil constrained in all degrees of freedom if C3D8I-elements are used in these regions and no external boundary conditions if the regions are modeled with CIN3D8-elements

    – Transverse load $T = 38.035$ kN and bending moment $M = 380.35$ kNm applied at the top of the wellhead via a reference point and a distributing coupling constraint

    – Gravity load ($g = 9.81$ m/s^2 in the negative y-direction) for the soil with the density ρ' specified

It is important to remember that the initial setup is the startup point for the parametric study and that a lot of the parameters will be varied and investigated to obtain an accurate finite element model as possible. It is also worth to point out that the finite element model for the three cases studied could be substantially different, because of the different soil compositions.

Regarding the combination of finite and infinite elements, the near-field region is modeled with C3D8I-elements whereas CIN3D8 is the element type in the far-field region, cf. Figure 3.14. In the far-field region, one infinite element in the radial direction was used. The lower region of the soil is also modeled with infinite elements and an element length of 5 meters was assumed to be reasonable. The mesh setup for the combination of finite and infinite elements is shown in Figure 3.15.
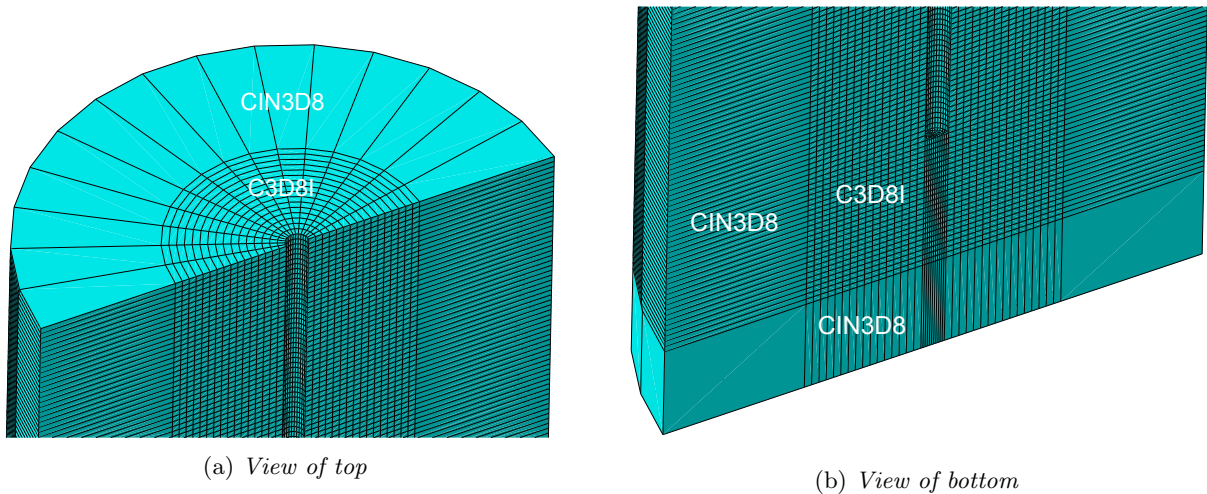

(a) *View of top*

(b) *View of bottom*

Figure 3.15: *Principal mesh setup for a combination of finite and infinite elements*

3.3.7 Parametric study

The parametric study will be carried out separately for each case studied because the effect of certain parameters is most likely dependent on the soil composition. A lot of parameters need to be investigated and the natural choice would be to start with the geometry and mesh of the soil.

CASE A

The first soil studied is a homogeneous stiff clay. With the help of Section 3.3.1, the following properties are used in the material model:

- $E_s = 60$ MPa

- $\nu = 0.45$

- $\varphi = 0°$

- $\psi = 0°$

- $c = s_u = 150$ kPa

The submerged unit weight of the stiff clay was determined to $\gamma' = 11.67$ kN/m^3 in Section 3.2, giving a density of $\rho' = 1190$ kg/m^3.

As mentioned above, a particular result of interest is the deformation at the top of the wellhead, just as when the soil was modeled with non-linear springs. The outer boundary of the soil should not affect the response of the wellhead. As a first step the effect of the soil radius on the deformation at the wellhead top was investigated. When modeling the soil with solely finite elements C3D8I and keeping the circumferential and lower boundary constrained, a radius of $18D$ and a length of 180 meters were considered sufficient to eliminate large boundary effects on the wellhead response. Here D refers to the outer diamater of the wellhead. These soil dimensions are considerably large leading to a lengthy computation. The deformation at the top was 7.759 mm.

For the model including only finite elements C3D8I, the von Mises equivalent stress for the wellhead is close to zero far away from the top, as it should be. However, even with the large soil dimensions the boundaries still affect the wellhead and therefore a model consisting of finite and infinite elements was investigated. After a lot of simulations with different dimensions of the soil and especially the radius of the near- and far-field region, an accurate response was obtained for the wellhead with a far-field radius of $11D$ and a near-field radius of $5.5D$ together with a length of the soil of 80 meters. The benefit of using infinite elements to simulate the infinite extent is evident, as the dimensions of the soil can be substantially smaller while still obtaining a realistic result. For this setup the global approximate mesh size was 0.25 meters and the deformation at the top of the wellhead was 7.739 mm, well in line with the result obtained from the model consisting of solely C3D8I-elements.

Regarding the von Mises equivalent stress for the wellhead, it is shown for both configurations in Figure 3.16. The stress is along an edge where $x = D/2$ and $z = 0$, meaning the outer surface of the wellhead.
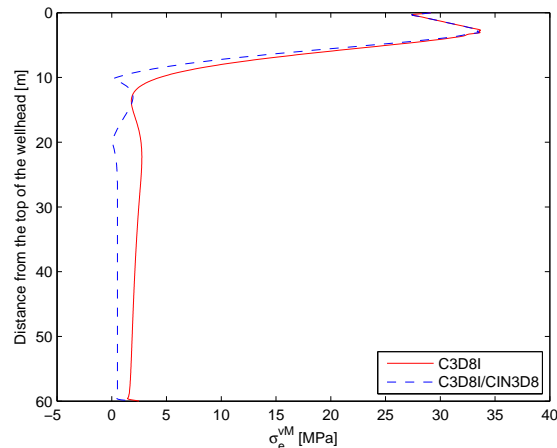

Figure 3.16: *von Mises equivalent stress for both configurations in case A*

The stress far away from the top of the wellhead is close to zero, as it should be. For the C3D8I/CIN3D8-model, the soil boundaries have in principle no effect on the wellhead response and the infinite elements are considered to simulate the infinite extent of the soil in an accurate way. Looking at the result from the C3D8I-model, the response is relatively accurate, but the soil boundaries affect the results slightly. This is due to the boundary conditions applied at the circumferential and lower boundary of the soil. The stress at the constrained boundaries are high, whereas for the C3D8I/CIN3D8-model the stress at the infinite boundaries are close to zero, as it should be in reality. Thus, in further analyses a combination of C3D8I- and CIN3D8-elements will be used.

With soil dimensions and mesh elements determined, the influence of the coefficient of friction in the tangential behavior for the contact between the outer surface of the wellhead and the surrounding soil was investigated. In the previous analyses a value of $\mu = 0.5$ was used. Three other coefficients of friction were evaluated and the deformation at the top of the wellhead is shown in Figure 3.13.

Table 3.13: Deformation at the top of the wellhead for different values of μ for case A

Coefficient of friction μ	Deformation [mm]
0	8.330
0.2	7.977
0.5	7.739
0.8	7.712

The von Mises equivalent stress for the wellhead was slightly affected by the coefficient of friction, whereas the deformation at the top changes substantially, as Table 3.13 shows. This is expected, lower friction between wellhead and soil means that the wellhead can move more freely in the soil, hence a larger deformation. As the coefficient of friction μ is unknown, a value of 0.5 is adopted but one should know that it has a large impact on the deformation at the top of the wellhead.

Another result of interest is the equivalent plastic strain $\bar{\epsilon}^{pl}$, defined as

$$\bar{\epsilon}^{pl} = \int \frac{1}{c} \boldsymbol{\sigma} : d\boldsymbol{\epsilon}^{pl} \tag{3.5}$$

where $\boldsymbol{\sigma}$ and $\boldsymbol{\epsilon}^{pl}$ is the stress and plastic strain tensor, respectively. For the finite element model consisting of a combination of C3D8I- and CIN3D8-elements and an approximate mesh size of 0.25 meters, the maximum equivalent plastic strain in the soil was $\bar{\epsilon}^{pl}_{max} = 0.005894$, occurring just at the sea bed. This is expected, as this region, because of the applied transverse load and bending moment at the top of the wellhead, is the most stressed leading to yielding of the soil.

CASE B

The second soil is a homogeneous soft clay with the following properties used in the material model when the soil is modeled as a continuum:

- $E_s = 25$ MPa
- $\nu = 0.45$
- $\varphi = 0°$
- $\psi = 0°$
- $c = s_u = 30$ kPa

The submerged unit weight of the soft clay was determined to $\gamma' = 10.01$ kN/m^3 in Section 3.2, giving a density of $\rho' = 1020$ kg/m^3.

Because of the advantage of using a combination of finite and infinite elements to model the soil seen in case A, analyses with only C3D8I-elements for the soft clay in case B were not carried out. Instead, the radius of the near- and far-field region and the length of the soil were investigated and it turned out for case B that the soil dimensions should be larger than those in case A to obtain an accurate wellhead response. This has to do with the rather low stiffness of the soft clay allowing for the wellhead to move more freely in the soil compared to the stiff clay. Nevertheless, a near-field radius of $9D$ and a far-field radius of $18D$ combined with a length of 80 meters for the soil were used in the finite element model. The von Mises equivalent stress at the outer surface of the wellhead is shown in Figure 3.17 with an approximate global mesh size of 0.2 meters.
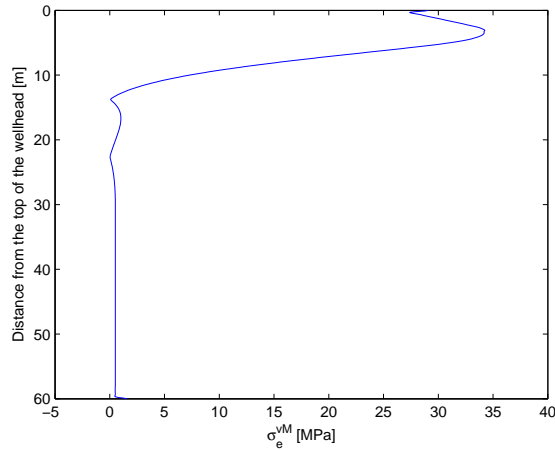
Figure 3.17: *von Mises equivalent stress for case B*

The stress is close to zero for large depths as expected. Compared with the stiff clay in case A (see Figure 3.16), the stress curve is similar, but with the exception of a non-zero stress for a larger part of the wellhead in case B. For this setup, the deformation at the top of the wellhead was 11.918 mm. A higher deformation for the soft clay compared to the stiff clay, as expected.

The effect of the coefficient of friction μ has been investigated and the results are displayed in Table 3.14.

Table 3.14: Deformation at the top of the wellhead for different values of μ for case B

Coefficient of friction μ	Deformation [mm]
0	13.034
0.2	12.316
0.5	11.918
0.8	11.823

Precisely as in case A, the wellhead von Mises equivalent stress is barely affected by the coefficient of friction. The deformation at the top of the wellhead increases with decreasing coefficient of friction, see Table 3.14. When varying the coefficient of friction, the deformation changes substantially and μ greatly affects the results.

Moving on to the equivalent plastic strain, the maximum value was $\bar{\epsilon}^{pl}_{max} = 0.052$ with a coefficient of friction of $\mu = 0.5$. This is almost ten times higher than the maximum plastic strain obtained for the stiff clay in case A, which is anticipated as the undrained shear strength for the soft clay is considerably smaller compared to the stiff clay, leading to a lower stress required before yielding. Also here the maximum equivalent plastic strain occurs just at the sea bed, in the soil closest to the wellhead.

CASE C

The last soil studied is a layered soil, see Figure 3.10. The properties for each soil layer are unique and the values used in the material model is shown in Table 3.15, where depth corresponds to the depth below the sea bed.

Table 3.15: Properties for each soil layer in case C

Depth [m]	Soil description	E_s [MPa]	ν	φ [°]	ψ [°]	c [kPa]	γ' [kN/m^3]	ρ' [kg/m^3]
0-5	Medium dense sand	60	0.35	33	3	1	9.01	918.4
5-10	Soft clay	20	0.45	0	0	20	10.01	1020
10-20	Stiff clay	65	0.45	0	0	80	10.84	1105
20-25	Stiff clay	70	0.45	0	0	100	11.34	1156
25-35	Dense sand	75	0.35	38	8	1	9.50	968.4
35-47	Soft clay	25	0.45	0	0	45	10.51	1190
47-bottom	Stiff clay	80	0.45	0	0	200	11.67	1071

42

Because of the inhomogeneous properties of the layered soil, the tangential behavior for the contact between the outer surface of the wellhead and the surrounding soil was assumed to be frictionless. In reality, every soil layer has a different value of μ and it is not correct to assume a constant value for each layer. Therefore, allowing the contact surfaces to slide freely against each other without friction was the most reasonable alternative.

Moving on to the mesh, no simulations were carried out with only C3D8I-elements and a combination of finite and infinite elements was employed from the beginning, just as for case B. A preliminary conclusion was that the computation time for the layered soil in case C was considerably longer compared to the other two cases due to the inhomogeneous properties. The near-field and far-field radius should be $5.5D$ and $11D$ respectively, together with a soil length of 80 meters. These dimensions are identical to the ones obtained in case A, and it is realistic as the average elastic stiffness of the layered soil is similar to that of the stiff clay in case A. To keep a short computation time, the approximate global mesh size was set to 0.3 meters. Figure 3.18 shows the von Mises equivalent stress at the outer surface of the wellhead.
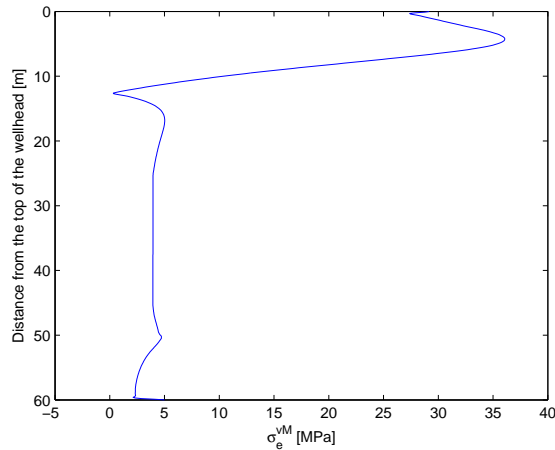

Figure 3.18: *von Mises equivalent stress for case C*

Overall the stress curve is accurate, but for large depths the stress is not zero, rather 5 MPa. This is believed to occur because of the different soil properties for the layered soil. The stiffness and density of each soil layer are different and therefore the stress in two different layers is substantially dissimilar, thus affecting the stress response of the wellhead. Worth noting is that the deformation at the top of the wellhead was 14.270 mm, which is actually higher compared to the soft clay. This has most likely to do with the sand present the first five meters below the sea bed. More analysis of the layered soil is carried out in Chapter 4.

Lastly, for the layered soil in case C the maximum equivalent plastic strain was found to be $\bar{\epsilon}^{pl}_{max} = 0.04665$, occurring close to the sea bed. Almost the entire first layer of sand has yielded and this is because of the low cohesion, cf. Table 3.15.

Additional analyses were carried out with the dilation angle ψ set to zero for both sand layers. There were some minor differences in the soil response, but the stress and deformation of the wellhead were identical. Hence, the dilation angle does not have a large influence on the results for the studied layered soil. One should keep in mind that in this case the dilation angle is small, 3° and 8° for the two sand layers, and larger values would most likely impact the simulations further.

3.3.8 Final comments

After studying the three cases, it is clear that the dimensions of the soil are dependent on the soil composition. A less stiff soil requires a larger soil radius and the required length of the soil solid half-cylinder is dependent on the unit weight and subsequently the density of the soil. When using a combination of finite and infinite elements, the soil dimensions can be lowered significantly, whilst still obtaining an accurate stress and deformation response for the wellhead. Another thing is the applied loads, if they would have been higher a larger soil radius would have been required to eliminate boundary effects.

The soft clay in case B requires largest soil dimensions, which is expected because of the large movement of the wellhead in the soft soil compared to the other two cases. However, the deformation at the top of the

wellhead was largest for case C, but this has to do with sand being the first layer in the soil studied. Overall, the deformations for the wellhead are largest in case B.

For the stiff and soft clay in case A and B, the coefficient of friction has a low influence on the wellhead stress response, but greatly influences the deformation at the top. Therefore, one has to be cautious when selecting a value of the coefficient of friction. To obtain an accurate response, the friction between the soil and wellhead should be determined experimentally.

The soil with the largest equivalent plastic strain is the soft clay in case B since its stiffness and undrained shear strength (cohesion) is low. For all three cases the maximum equivalent plastic strain is close to the sea bed, in the soil closest to the wellhead. In case A and B, the response in the soil is mostly linear, except for the yield region close to the sea bed. For case C, most regions of the soil have undergone plastic deformation, with yielding in almost the entire first layer of sand.

In the parametric study above for the three cases, no investigations about Young's modulus or Poisson's ratio have been carried out. This has to do with the fact that the values were selected with the help of Table 3.11 above and the focus of the continuum soil modeling is not on the actual numerical values of the wellhead stress or deformation, but rather how the results are affected by different parameters in the finite element model. For a homogeneous soil, it is obvious that a lower stiffness leads to larger deformations.

4 Comparison between soil modeling methods

In this chapter the results from the two soil modeling strategies will be compared and discussed. The comparison is carried out for each case separately and the optimal configuration for the two modeling strategies will be compared against each other. For the non-linear springs modeling strategy, all results below is for the outer surfaces coupling type, cf. Section 3.2. At the end of the chapter advantages and disadvantages for the two modeling strategies are presented.

4.1 Case A

For the homogeneous stiff clay, the deformation and the von Mises equivalent stress response for the wellhead are shown in Figure 4.1.

(a) *von Mises equivalent stress* (b) *Deformation*
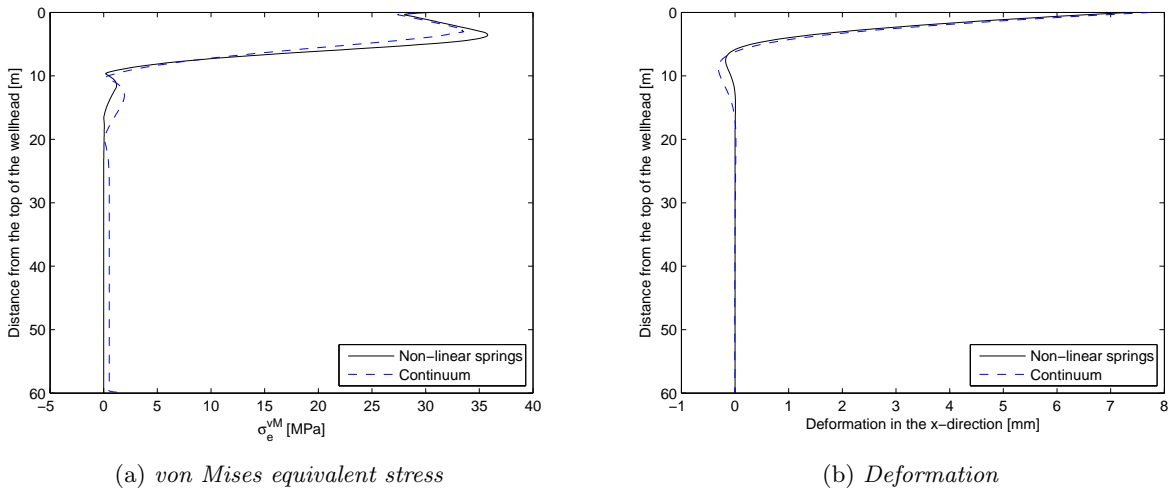
Figure 4.1: *Case A: wellhead response for the two modeling strategies*

Overall the shape of the deformation and stress curve is similar for the two modeling strategies, but with some differences. The largest deformation of the soil is close to the sea bed as expected, and for the first non-linear spring located 0.5 meters below the sea bed the lateral deflection is 1.474 mm because of the transverse load and bending moment. For the first spring, the maximum lateral resistance P occurs for a lateral deflection of 5 mm, see Figure 2.7. In the figure it can be seen that for a lateral deflection y below the maximum lateral resistance, the $P - y$ curve is somewhat linear. Because of the low deflection for the first spring, the soil response is in the linear region when it is modeled with non-linear springs and $P - y$ curves. This was also seen for continuum soil modeling, where the response was mainly linear with some yielding in the soil at the sea bed, closest to the wellhead. The deformation in x-direction for the soil closest to the wellhead 0.5 meters below the wellhead was 1.752 mm, which is close to the value obtained for non-linear springs soil modeling.

As the soil response is mainly linear, Young's modulus E_s for the soil has a large impact on the results. From the $P - y$ curves for stiff clay, as the lateral deflection is in the linear region, an approximate value of E_s can be found by calculating the slope of the $P - y$ curves. It was estimated to 100 MPa, and in continuum soil modeling a value of 60 MPa was used, hence the differences in the results between the two modeling strategies. Worth noting is that the lateral deflection at the top of the wellhead was 7.348 mm and 7.739 mm for non-linear springs and continuum modeling, respectively. The deformation for the two strategies is similar, but one should keep in mind that it is affected by not only the stiffness, the coefficient of friction also has an influence, as was seen in Section 3.3.7.

4.2 Case B

The deformation and the von Mises equivalent stress response for the wellhead when the soil was assumed to be a homogeneous soft clay are shown in Figure 4.2.
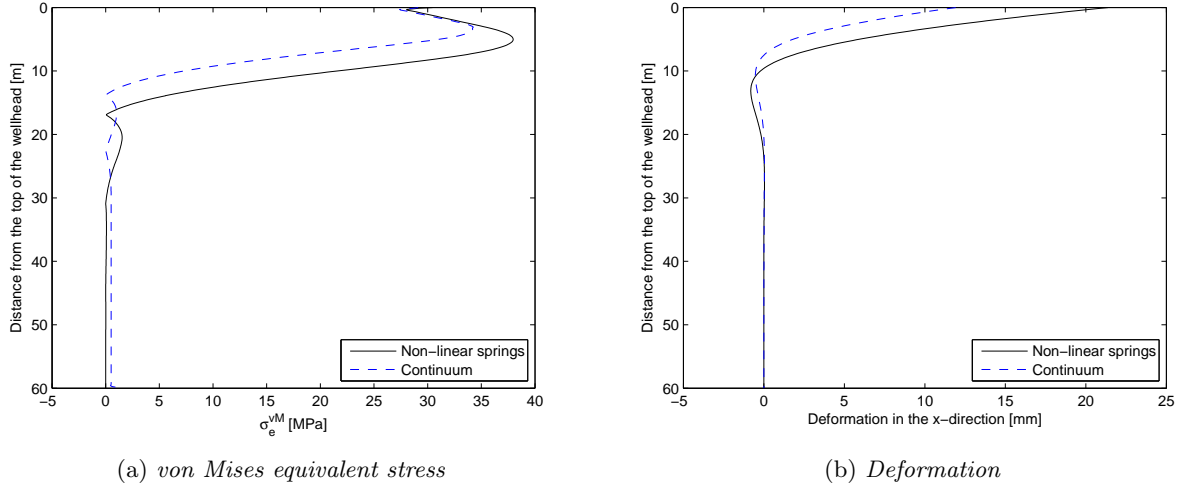

(a) *von Mises equivalent stress* (b) *Deformation*

Figure 4.2: *Case B: wellhead response for the two modeling strategies*

Just as for case A, the wellhead deformation and stress response is similar for both modeling strategies, but with some numerical differences. Modeling the soil with non-linear springs, the lateral deflection of the first spring (located 0.5 meters below the sea bed) was 9.618 mm, whereas the deflection was 3.909 mm for the continuum soil modeling method. Just as for the stiff clay, the response for the soft clay is mainly linear and for the first soil spring the lateral resistance P is about one third of the maximum lateral resistance, cf. Figure 2.5. For this initial portion of the $P - y$ curve, E_s was estimated to 4 MPa, and when modeling the soil as a continuum, a value of $E_s = 25$ MPa was employed for the soft clay. This explains the differences in the results above, as the deformation and stress are larger for non-linear springs modeling compared to continuum modeling. The deformation at the top of the wellhead was 21.372 mm when using lateral soil springs, and 11.918 mm when the soft clay was modeled as a continuum, and the variation in results is a direct consequence of the stiffness of the soil. As expected, the coefficient of friction between the soft clay and the wellhead used in continuum soil modeling also has an influence on the wellhead deformation, as was seen in Section 3.3.7. Worth noting is that the yielding of the soft clay occurs in the same area as for the stiff clay in case A, but in a larger region which is expected because of the difference in undrained shear strength or cohesion for the two studied clays.

4.3 Case C

The wellhead stress and deformation response for the layered soil in the third case are shown in Figure 4.3.

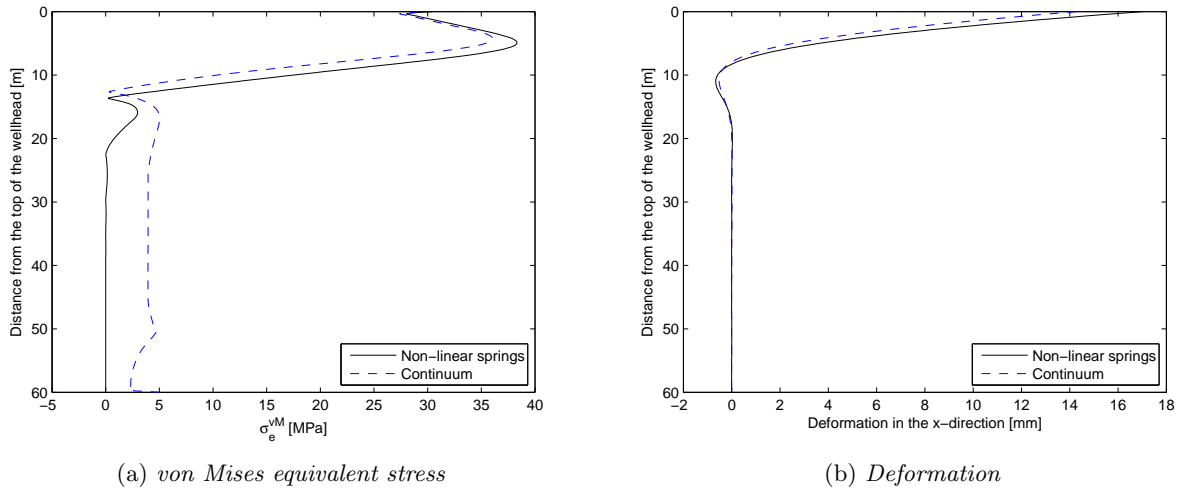(a) *von Mises equivalent stress*

(b) *Deformation*

Figure 4.3: *Case C: wellhead response for the two modeling strategies*

The layered soil in case C is hard to analyze but the shape of the deformation and stress curve is similar for both modeling strategies, especially the deformation. As for the stress, it is non-zero at large depths when the soil is modeled as a continuum. This is due to each soil layer having different properties. Because of the applied gravity load, there are some discontinuities in the stress of the soil, as each soil layer has a unique density. This is transferred to the wellhead, explaining the high stresses far away from the wellhead top, cf. Figure 4.3a. This is not an issue for the deformation, and the two modeling strategies give similar results, see Figure 4.3b.

When the layered soil is modeled with non-linear springs the lateral deflection of the first soil spring located 0.5 meters below the sea bed was 6.696 mm and for continuum soil modeling the deformation in x-direction was 5.133 mm. From the $P - y$ curve for the first soil spring located in the sand layer E_s was estimated to 5 MPa, and a value of 60 MPa was used for the medium dense sand in the first soil layer when the soil was modeled with solid elements. Subsequently, the deformation of the wellhead should be lower in continuum modeling, as is seen in Figure 4.3b. The deformation at the top of the wellhead for non-linear springs is 17.012 mm and for continuum soil modeling 14.270 mm.

There is a large difference in stiffness for the two modeling strategies, but both the deformation of the soil and the wellhead is similar. This is due to the fact that almost the entire first sand layer has yielded, because of the low cohesion used in continuum soil modeling, cf. Table 3.15. One should also keep in mind that the outer surface of the wellhead and the surrounding soil were assumed to slide freely against each other without friction. If friction between these surfaces is included in the continuum soil model, the deformation would surely be affected, just as in case A and B.

4.4 Additional comments

For the stiff clay in case A the wellhead response is similar for both modeling strategies. This is due to the fact that the lateral deformation of the soil is small and it is a good approximation to assume elastic-perfectly plastic behavior for the continuum soil modeling. On the other hand, if the lateral deflection of the soil would have been so large that softening occurs, cf. Figure 2.7, the differences between the two modeling strategies would have been more substantial. Assuming elastic-perfectly plastic behavior for large deformations of stiff clay subjected to static loading is not a reliable assumption, and the inelastic behavior must be characterized in a more accurate way for continuum soil modeling.

For soft clay and sand an elastic-perfectly plastic relationship for the soil is reasonable for static loading, see Figures 2.5 & 2.10. For both soil types the initial relationship between the lateral resistance P and the lateral deflection y is linear, and for large deflections the lateral resistance is constant. This is similar to an elastic-perfectly plastic model, where hardening or softening of the soil is neglected. In case B, the response is mainly linear and the differences between the two modeling strategies mostly arise because of the soil stiffness. If a lower value of E_s had been specified for the soft clay in continuum modeling, the wellhead response would have been closer to the one obtained for non-linear springs modeling.

47

After studying case C, it can be concluded that analysis of a layered soil is much simpler using non-linear springs compared to continuum modeling. As was stated above, the properties in each soil layer are unique leading to discontinuities in the soil stress response, just at the interface between two soil layers. These discontinuities are transferred to the wellhead stress response, leading to an inaccurate response in continuum soil modeling, see Figure 4.3a. In the figure the wellhead stress response for non-linear springs modeling is also seen, which is realistic. Worth noting is that the deformation for the two modeling strategies is similar.

4.5 Advantages and disadvantages for the two modeling strategies

After studying the three different cases advantages and disadvantages for the two soil modeling strategies have been identified and summarized. All simulations have been carried out for static loading, but here cyclic loading is covered as well. In Table 4.1 the assessment of non-linear springs soil modeling is seen.

Table 4.1: Advantages and disadvantages when modeling the soil with non-linear springs and $P - y$ curves

Advantages	Disadvantages
+ Simple finite element model + Short computation time + Both elastic and inelastic soil behavior incorporated in the $P - y$ curves + Few material parameters	– Requires external $P - y$ curves – One-dimensional soil behavior – Spring discretization and attachment type greatly influence the results – Repetitive modeling if no external script is used – No possibility of modeling time-dependent behavior such as creep, consolidation or irreversible plastic strains – Restricted to pile-soil interaction

The strength of non-linear springs with $P - y$ curves to model the soil lies in the method's simplicity and the short computation time. However, for cyclic loading there are some limitations to the method, especially the complete disregard to irreversible plastic strains. Moving on, in Table 4.2 the evaluation of modeling the soil as a continuum is displayed.

Table 4.2: Advantages and disadvantages when modeling the soil as a continuum with solid elements

Advantages	Disadvantages
+ Easy to switch soil type + Can account for time-dependent long-term effects + Possibility to employ advanced constitutive models for the inelastic behavior + Three-dimensional soil behavior with the opportunity to account for anisotropy + Soil interaction with arbitrary structure can be modeled	– Complex finite element model – Long computation time – Requires additional material parameters compared to $P - y$ curves – Results greatly influenced by a number of factors, such as soil dimensions, mesh and contact properties

The finite element model for continuum soil modeling is complex and there are a lot more parameters that affect the results compared to non-linear springs soil modeling. This leads to a long computation time, i.e. expensive simulations. The strength of the method is the possibility to employ advanced constitutive models for the inelastic behavior and to be able to predict long-term effects of cyclic loading.

5 Concluding remarks and future work

Using non-linear springs together with $P - y$ curves is a simple approach to model soil-structure interaction when the structure is subjected to lateral loads. The non-linear behavior of the soil is incorporated in the $P - y$ curves and they can easily be computed for various types of soil, as was seen in Section 2.4. The commercial software LPILE used to compute $P - y$ curves can without difficulty be replaced by a MATLAB-script, thus saving license money. A drawback of the current MATLAB-script developed for this thesis is that the layered soil approach, cf. [25], is not implemented and for future work this should be prioritized, as all soils in reality are more or less inhomogeneous.

Connecting the springs to the structure is simple and the computation time is short. In Abaqus/CAE, using a Python-script to create the finite element model is preferred to avoid repetitive work and to be able to easily switch between different soil types and spring discretizations. As was shown in Section 3.2, the non-linear springs should be connected to the outer surface of the structure in order to obtain an accurate stress response, whereas the deformation is not affected by the attachment type. In the same section it was also determined that an optimal discretization of springs is highly dependent on the soil composition, and this must be taken into consideration when determining the placement of soil springs.

The wellhead stress and deformation response is considered accurate when the soil is modeled with non-linear springs. However, the complex three-dimensional behavior of the soil is not taken into account by the lateral soil springs. Additional springs with other degrees of freedom could be added to the model, e.g. axial or rotational springs, cf. [23]. This increases the complexity of the model and the behavior of the new springs must be matched to the soil's expected behavior. In the simple load case studied, lateral soil springs with $P - y$ curves should be sufficient to obtain an accurate response for short-term static loading, as stated in [2].

A problem with the use of non-linear springs for long-term effects is that phenomena such as creep or consolidation cannot be taken into account. Another limitation by using springs is that yielding cannot be modeled. The non-linear behavior is incorporated in the $P - y$ curves, but if the soil is yielding during loading and when removing the load, then irreversible plastic strains should be present in the soil. This is not included in the $P - y$ curves and during unloading the soil is assumed to be completely unstrained. Another drawback of using $P - y$ curves for cyclic loading is that the behavior of the soil is independent of the nature of the load. No consideration is taken to e.g. cycle time, stress amplitude or stress ratio, and the lateral behavior of the soil is considered to be equal for all types of cyclic loads, see Appendix A. This is surely an inaccurate assumption, and to accurately predict long-term effects of soil-structure interaction, continuum soil modeling should be used.

When modeling soil as a continuum using solid elements, the most important part is the material model and in particular the mechanical properties of the soil. A pertinent constitutive model to predict the inelastic behavior of the soil is required. As soils are highly non-linear, the constitutive model largely influences the results. Other important factors are the dimensions and mesh of the soil in the finite element model. In Section 3.3 this was clearly seen, and a combination of finite and infinite elements should be used when modeling the soil. When only finite elements are used to model the soil, the dimensions of the outer boundary have to be significantly large to eliminate artificial soil boundary effects on the wellhead response. If infinite elements are used, it is important to have a large enough far-field radius of the soil to invoke zero displacements at the infinite boundaries. The required dimensions are highly dependent on soil composition and applied load. Furthermore, no mesh convergence studies were carried out in this thesis but it is an interesting topic for future continuum soil analyses.

Continuum soil modeling is more complex and time-consuming compared to non-linear springs modeling. The simulation time is long, especially for a layered soil. The benefit of modeling the soil as a continuum is that long-term effects such as consolidation and creep can be included in the finite element model. Also, hardening or softening of the soil can be specified and this is especially interesting when studying soil-structure interaction for cyclic loading. The complex three-dimensional behavior of a soil is accounted for and anisotropic behavior can even be specified, which is not possible for the one-dimensional lateral soil springs. From the three soil compositions studied in this thesis, it can be concluded that an accurate finite element model is unique for each soil type, which leads to a long optimization process in terms of modeling.

For the static short-term analysis considered in this thesis, the wellhead stress and deformation responses are similar for both modeling strategies, especially for the two homogeneous soils. There are some differences in the stress response though, and this has mainly to do with the chosen material parameters and in particular the elastic stiffness, since the response is mainly linear. For the layered soil the deformation of the wellhead is in agreement for continuum and non-linear springs modeling. The stress on the other hand is substantially

different, with non-linear springs giving the most reasonable response. Continuum soil modeling of a layered soil is complicated because of the unique properties in each soil layer, and subsequently the finite element model is highly sensitive to parameter changes. To further complicate the analysis of a continuum layered soil, the contact properties are different for the different layers. The contact properties in general need to be investigated, especially the coefficient of friction as it has a large impact on the deformation of the wellhead, as was seen in Section 3.3.7.

When studying static loading, non-linear springs should be used to model the soil due to their simplicity. For cyclic loading continuum soil modeling is preferred because of the ability to predict long-term effects such as creep, consolidation and plastic strains, which is not included in $P - y$ curves. A continuum model is however complicated and future work should focus on determination of a soil's material parameters, both elastic and plastic ones, and how to model creep and consolidation, if these two phenomena are of interest. In this thesis a constitutive model of Mohr-Coulomb type has been used to predict the inelastic behavior of the soil, and other plasticity models are available in Abaqus/CAE, such as Drucker-Prager and Cam clay. The different constitutive models should be analyzed to determine which is the most applicable one for the considered soil and loading case.

Moving on, Abaqus has been used exclusively in this thesis and an undrained analysis (cf. Section 2.3.5) of the soil was carried out. The possibility to use effective strength parameters for the inelastic behavior is a topic of interest for future work, meaning a drained analysis of the soil. According to [5], a drained analysis is more accurate than an undrained analysis, but it is more complicated because the effective or drained strength parameters need to be determined experimentally and the pore water pressure present in the soil must be known prior to the analysis.

A commercial software that is used extensively in industry for continuum soil modeling is PLAXIS, which includes advanced constitutive models for the simulation of the non-linear and time-dependent behavior of soils, see [12]. PLAXIS is intended for analysis of deformation and stability of soil structures and for future continuum soil modeling the use of PLAXIS is definitely interesting.

In this thesis a simplified model of the complete wellhead assembly has been used and future analyses of continuum soil modeling should be carried out with the whole structure in the simulations. However, for the wellhead assembly the computation time when using non-linear springs to model the soil is long as it is, and modeling the soil as a continuum is more than likely too computationally expensive.

To summarize, soil-structure interaction is a difficult subject, mainly because of the complex mechanical behavior of soils. The results are greatly influenced by the properties of the soil and it is crucial that these are determined accurately through field or laboratory experiments on soil samples. This thesis has showed that modeling the soil as a continuum is possible, but the finite element model quickly becomes complex and the simulations are expensive compared to modeling the soil with non-linear springs. In static analyses, modeling the soil with non-linear springs and $P - y$ curves is the best strategy because of the method's simplicity. For cyclic loading, soil springs could be utilized as well, but one should be aware of the limitations that come with $P - y$ curves, such as no possibility to account for creep, consolidation or irreversible plastic strains. If these phenomena are of particular interest, continuum soil modeling is without a doubt a viable alternative to non-linear springs.

Bibliography

[1]   J. Wolf. *Dynamic Soil-Structure Interaction.* Prentice-Hall International Series in Civil Engineering and Engineering Mechanics. Prentice-Hall, 1985. ISBN: 9780132215657.

[2]   G. Grytøyr, T. Hørte, and A. Lem. *Wellhead Fatigue Analysis Method.* Technical report 2011-0063. Det Norske Veritas AS, 2011-01-18.

[3]   API RP 2A-WSD. *Recommended Practice for Planning, Designing and Constructing Fixed Offshore Platforms — Working Stress Design.* American Petroleum Institute, October, 2010.

[4]   T. Spink. *Geotechnical and Geoenvironmental Software Directory.* 2014. URL: http://www.ggsd.com.

[5]   S. Helwany. *Applied Soil Mechanics with Abaqus Applications.* Hoboken, New Jersey, USA: John Wiley and Sons, 2007. ISBN: 9780471791072.

[6]   A. Verruijt. *Soil Mechanics.* Delft, the Netherlands: Delft University of Technology, 2012.

[7]   A. Verruijt. *Offshore Soil Mechanics.* Delft, the Netherlands: Delft University of Technology, 2012.

[8]   C. S. Desai and M. Zaman. *Advanced Geotechnical Engineering: Soil-Structure Interaction using Computer and Material Models.* Boca Raton, Florida, USA: CRC Press, 2013. ISBN: 9781466515604.

[9]   R. F. Craig. *Craig's Soil Mechanics.* New York, USA: CRC Press, 2004. ISBN: 9780415327022.

[10] J. E. Bowles. *Foundation Analysis and Design.* 5th edition. New York, USA: McGraw-Hill, 1996. ISBN: 9780071140522.

[11] H. Jiang and Y. Xie. A Note on the Mohr–Coulomb and Drucker–Prager Strength Criteria. *Mechanics Research Communications* **38**.4 (2011), 309–314. ISSN: 0093-6413.

[12] Plaxis bv. *PLAXIS 2D Manual.* 2014. URL: http://www.plaxis.nl.

[13] L. Reese and S.-T. Wang. *COM624P — Laterally Loading Pile Analysis Program for the Microcomputer.* Technical report FHWA-SA-91-048. Version 2.0. US Department of Transportation, Federal Highway Administration, June, 1993.

[14] H. Matlock. Correlations for Design of Laterally Loaded Piles in Soft Clay. *Proceedings of the 2nd annual Offshore Technology Conference, Paper No. OTC 1204* (April, 1970).

[15] L. Reese, W. Cox, and F. Koop. Field Testing and Analysis of Laterally Loaded Piles in Stiff Clay. *Proceedings of the 7th annual Offshore Technology Conference, Paper No. OTC 2312* (April, 1975).

[16] L. Reese, W. Cox, and F. Koop. Analysis of Laterally Loaded Piles in Sand. *Proceedings of the 6th annual Offshore Technology Conference, Paper No. OTC 2080* (April, 1974).

[17] ANSYS Inc. *ANSYS 14.5 Workbench Help.* 2013. URL: http://www.ansys.com.

[18] L. Reese et al. *LPILE Plus 5.0 for Windows: Technical Manual.* July, 2004.

[19] M. O'Neill and J. Murchison. *An Evaluation of P-y Relationships in Sand.* Technical report PRAC 82-41-1. Houston, Texas, USA: University of Houston, March, 1983.

[20] M. Ashour and G. Norris. Modeling Lateral Soil-Pile Response Based on Soil-Pile Interaction. *Journal of Geotechnical and Geoenvironmental Engineering* **126**.5 (2000), 420–428. ISSN: 1090-0241.

[21] L. Reese and W. Van Impe. *Single Piles and Pile Groups Under Lateral Loading.* London, United Kingdom: CRC Press, 2000. ISBN: 9789058093486.

[22] F. Li and H. Tang. Simulation and Analysis for Laterally Loaded Pile in Clay. *Applied Mechanics and Materials* **90-93** (2011), 580–583. ISSN: 1660-9336.

[23] ISO 19902:2007(E). *Petroleum and Natural Gas Industries — Fixed Steel Offshore Structures.* International Organization for Standardization, 2007-12-01.

[24] R. Whitehouse. *Scour at Marine Structures: A Manual for Practical Applications.* London, United Kingdom: Thomas Telford Publishing, 1998. ISBN: 9780727726551.

[25] M. Georgiadis. Development of P-y Curves for Layered Soils. *Proceedings of the Conference on Geotechnical Practice in Offshore Engineering* (April, 1983).

[26] DNV-RP-C203. *Fatigue Design of Offshore Steel Structures — Recommended Practice.* Det Norske Veritas AS, October, 2012.

[27] Dassault Systemes Simulia Corporation. *Abaqus 6.13 Documentation.* 2013. URL: http://50.16.176.52/v6.13/.

[28] L. Reese et al. *LPILE Plus 5.0 for Windows: User's Manual.* July, 2004.

[29] M. Gu et al. Response of 1x2 Pile Group under Eccentric Lateral Loading. *Computers and Geotechnics* **57** (2014), 114–121. ISSN: 0266-352X.

[30] Y. Kim and S. Jeong. Analysis of Soil Resistance on Laterally Loaded Piles Based on 3D Soil–Pile Interaction. *Computers and Geotechnics* **38**.2 (2011), 248–257. ISSN: 0266-352X.

Appendices

A Computation of $P - y$ curves for cyclic loading

The method to produce $P - y$ curves for static loading was presented in Section 2.4.2, and here cyclic loading is covered. For the computations that are equal for both static and cyclic loading, the reader is referred to aforementioned section.

A.1 Soft clay

For cyclic loading the $P - y$ curve is produced in the same manner as for static loading for values of P less than 72% of P_u. The intersection between Equations 2.12 and 2.13 defines the transition depth X_R. If the undrained shear strength s_u and submerged unit weight γ' are constant with depth, the transition depth X_R is given by

$$X_R = \frac{6 s_u D}{\gamma' D + J s_u} \tag{A.1}$$

How the $P - y$ curve is produced for cyclic loading is dependent on the actual depth X. If the actual depth is greater than or equal to the transition depth, i.e. $X \geq X_R$, the $P - y$ curve is produced as

$$P = \begin{cases} 0.5 P_u \left(\frac{y}{y_{50}} \right)^{\frac{1}{3}} & 0 \leq y \leq 3 y_{50} \\ 0.72 P_u & y > 3 y_{50} \end{cases} \tag{A.2}$$

On the other hand, if the actual depth is less than the transition depth ($X < X_R$), the $P - y$ curve is computed as

$$P = \begin{cases} 0.5 P_u \left(\frac{y}{y_{50}} \right)^{\frac{1}{3}} & 0 \leq y \leq 3 y_{50} \\ 0.06 P_u \left[\left(\frac{X}{X_R} - 1 \right) \left(\frac{y}{y_{50}} - 3 \right) + 12 \right] & 3 y_{50} < y \leq 15 y_{50} \\ 0.72 P_u \left(\frac{X}{X_R} \right) & y > 15 y_{50} \end{cases} \tag{A.3}$$

For cyclic loading, a typical $P - y$ curve for soft clay is shown in Figure A.1.
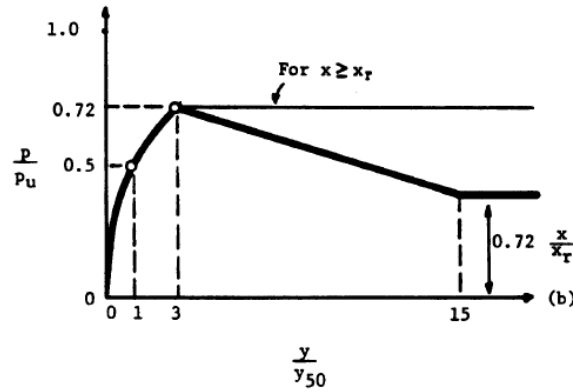

Figure A.1: *Characteristic shape of a $P - y$ curve for soft clay (cyclic loading), from [14]*

A.2 Stiff clay

For cyclic loading the first step is to compute a reference point y_p as

$$y_p = 4.1 A_s y_{50} \tag{A.4}$$

With the reference point calculated, the $P - y$ curve is constructed in a piecewise manner, just as for static loading

$$P = \begin{cases} k_c X y & y \leq y_{int} \\ A_c P_c \left[1 - \left| \frac{y - 0.45 y_p}{0.45 y_p} \right|^{2.5} \right] & y_{int} < y \leq 0.6 y_p \\ 0.936 A_c P_c - \frac{0.085}{y_{50}} P_c (y - 0.6 y_p) & 0.6 y_p < y \leq 1.8 y_p \\ 0.936 A_c P_c - \frac{0.102}{y_{50}} P_c y_p & y > 1.8 y_p \end{cases}$$ (A.5)

Here y_{int} is the intersection point between the first two equations defined in A.5. If the point does not exist, the first equation defines the whole $P - y$ curve, i.e.

$$P = \left\{ k_c X y \quad \forall y \right.$$ (A.6)

For stiff clay subjected to cyclic loading, a representative $P - y$ curve is displayed in Figure A.2, when assuming there is an intersection point y_{int}.
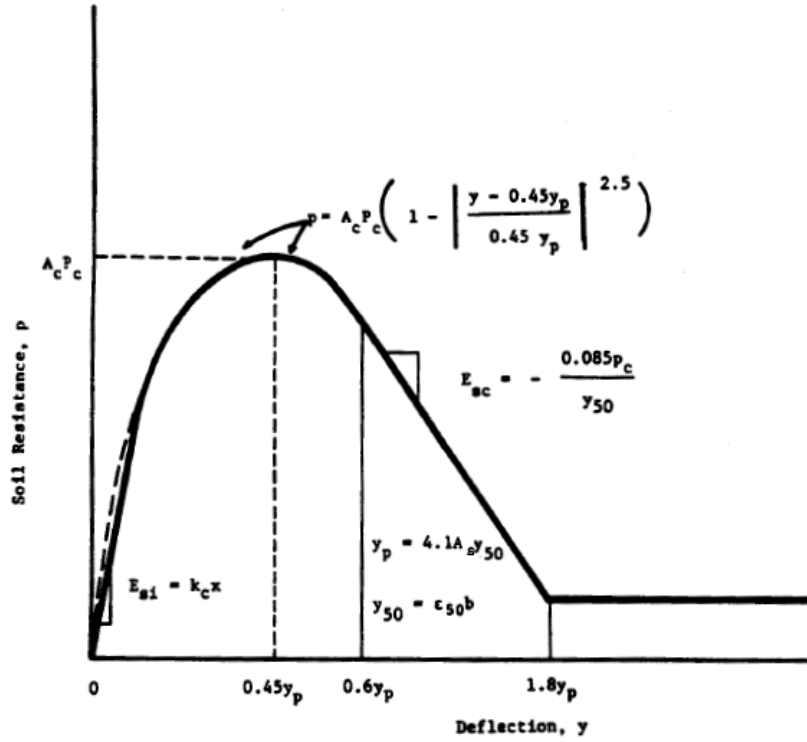
Figure A.2: *Characteristic shape of a $P - y$ curve for stiff clay (cyclic loading), from [15]*

B   Validation of $P - y$ curves

In this appendix the created MATLAB script to produce $P - y$ curves is validated against a commercial software named LPILE, see [4].

The MATLAB script is written in such a way that it is only possible to obtain a $P - y$ curve for one soil layer at a time, or for homogeneous soils. If one is studying a layered soil, the approach proposed in [25] is employed in LPILE but not in MATLAB. As of now, this is not included in MATLAB, but according to [28] the layered soil approach has little or sometimes no influence on the $P - y$ relationship for clay and it was disregarded in the implementation in MATLAB.

The validation has been carried out in such a way that representative material parameters for soft clay, stiff clay and sand have been chosen and the results from MATLAB and LPILE was compared, both for static and cyclic loading. The pile diameter was constant and equal to $D = 1$ m.

B.1   Soft clay

When comparing the response of soft clay, the following representative material parameters were used:

- $s_u = 20$ kPa

- $\gamma' = 30$ kN/m^3

- $\epsilon_{50} = 0.02$

The resulting $P - y$ curves obtained in MATLAB and LPILE for both static and cyclic loading for different depths X are shown in Figures B.1 & B.2.
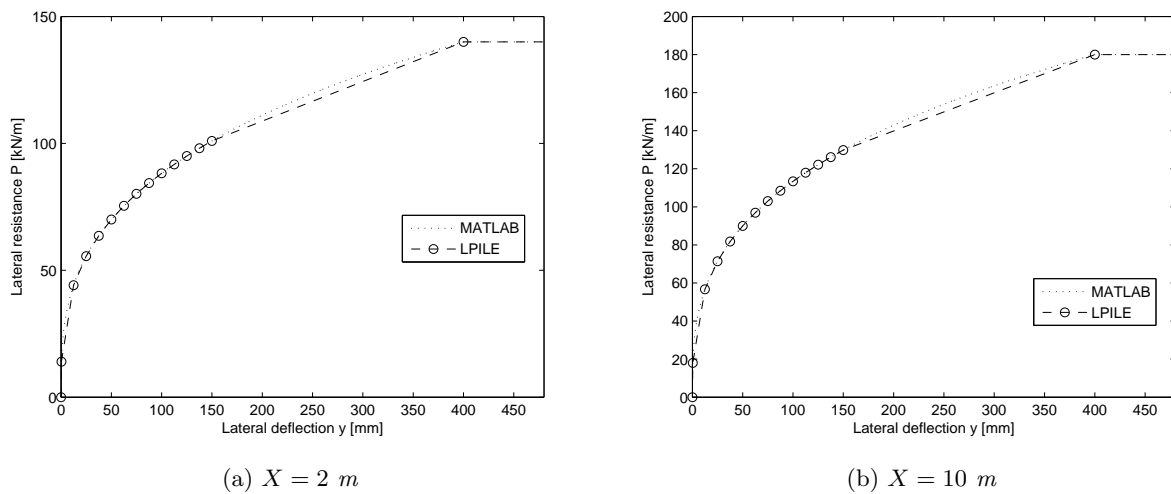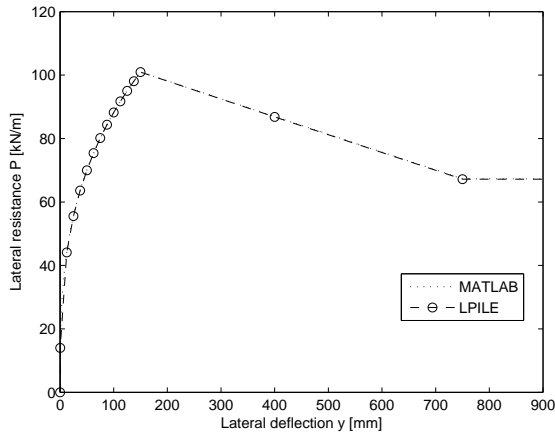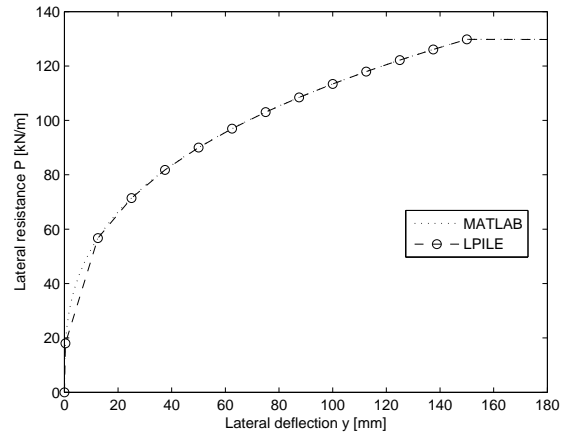

(a) $X = 2\ m$ (b) $X = 10\ m$

Figure B.1: $P - y$ curves for a representative soft clay subjected to static loading

(a) $X = 2\ m$

(b) $X = 10\ m$

Figure B.2: $P - y$ curves for a representative soft clay subjected to cyclic loading

We can see that the curves obtained from MATLAB and LPILE are in fact identical and the implementation for constructing $P - y$ curves for soft clay in MATLAB can be considered correct. Fewer points are used in LPILE to generate the $P - y$ curve which explains the small differences seen in the figures above.
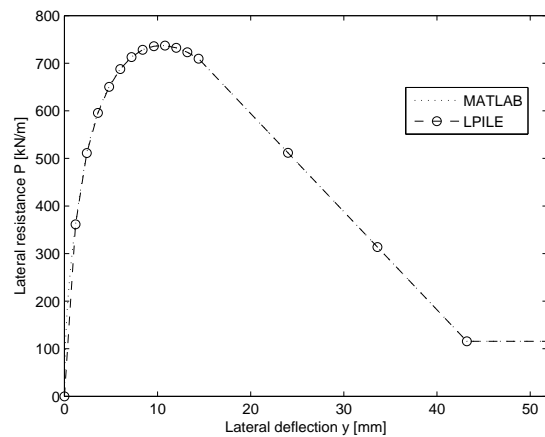
B.2 Stiff clay

Moving on to stiff clay, the following representative material parameters were used for the validation:

- $s_u = s_a = 120$ kPa

- $\gamma' = 50$ kN/m^3

- $\epsilon_{50} = 0.004$

The $P - y$ curves obtained in MATLAB and LPILE are displayed in Figures B.3 & B.4.
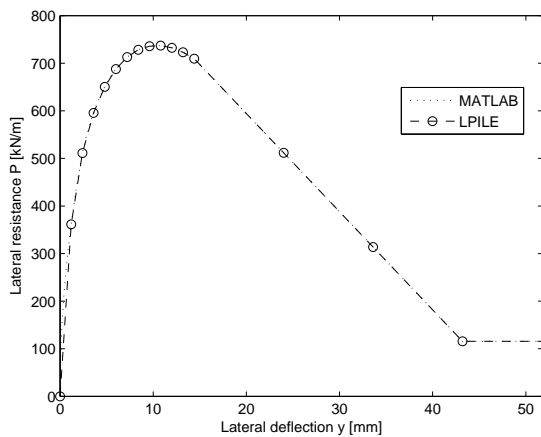
(a) $X = 5\ m$

(b) $X = 15\ m$

Figure B.3: $P - y$ curves for a representative stiff clay subjected to static loading
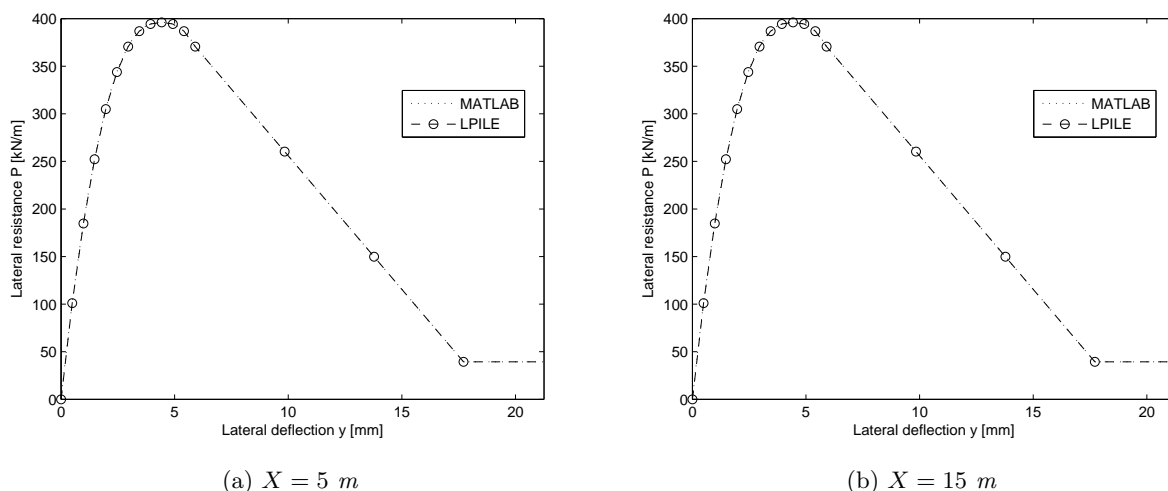
(a) $X = 5\ m$ (b) $X = 15\ m$

Figure B.4: $P - y$ curves for a representative stiff clay subjected to cyclic loading

Also for stiff clay the two computed $P - y$ curves are equal. Notice also that the $P - y$ curve is not changing with depth X. This is due to the fact that for $X = 5$ m the depth dependence on the ultimate soil resistance P_c have already vanished, see Equations 2.16 & 2.17. Additional comparisons have been carried out at low depths and there was still a good correlation between MATLAB and LPILE.

B.3 Sand

The last validation concerns sand and because of the many material parameters needed to define sand, two types of representative sand have been examined. The first representative sand had the following material parameters:

- $\gamma' = 10$ kN/m^3

- $\varphi = 31°$

- $k = 16300$ kPa/m

The computed $P - y$ curves in MATLAB and LPILE for the first representative sand are shown in Figure B.5.

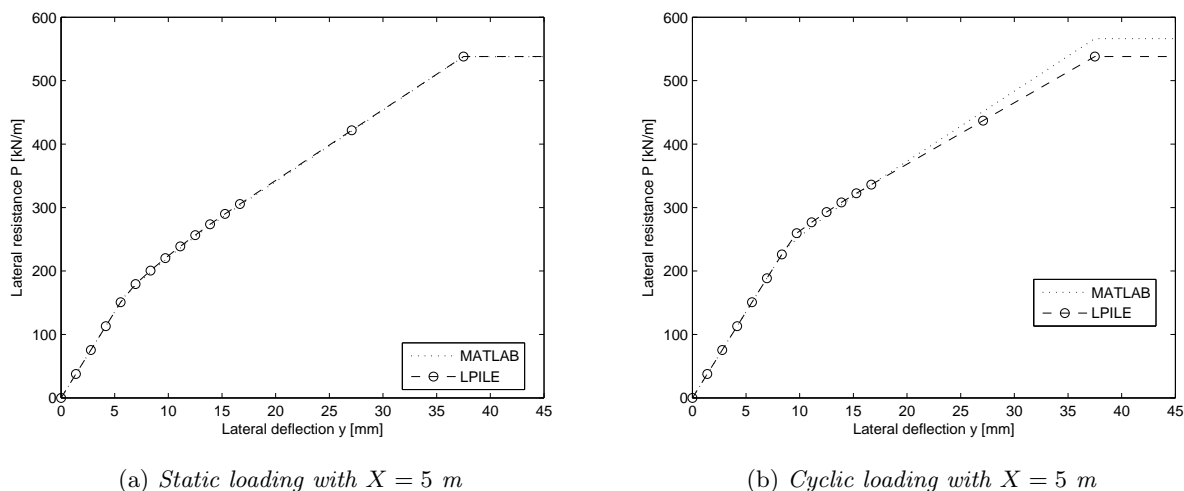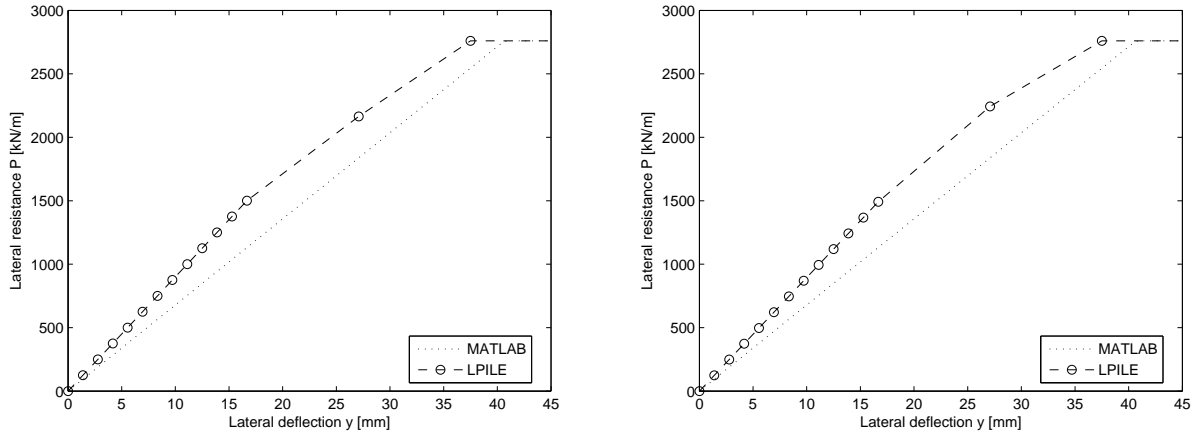(a) Static loading with $X = 5\ m$ (b) Cyclic loading with $X = 5\ m$

Figure B.5: $P - y$ curves for the first representative sand

The second representative sand was chosen to have the following material parameters:

VI

- $\gamma' = 16 \text{ kN/m}^3$

- $\varphi = 25°$

- $k = 5430 \text{ kPa/m}$

In Figure B.6 the obtained $P - y$ curves are displayed.

(a) *Static loading with $X = 12.5 \ m$* (b) *Cyclic loading with $X = 12.5 \ m$*

Figure B.6: *$P - y$ curves for the second representative sand*

Compared to soft and stiff clay, the difference between MATLAB and LPILE for sand is more substantial. Overall there is a good correlation between the two methods, and the differences seen in the figures above arise because of the initial soil modulus k and because of LPILE taking layered soils into account. The friction angle and denseness of the sand was used to determine k (see Table 2.3 above) and LPILE might use another way of determining k. Also, when producing the $P - y$ curves in LPILE, a layered soil with two sand layers was generated, meaning that the second layer is affected by the overlying first layer. This is not taken into consideration in MATLAB as stated above, but the results clearly show that for the second representative sand, the $P - y$ curves computed in MATLAB are similar to the ones obtained in LPILE.

B.4   Conclusions

For soft and stiff clay the computed $P - y$ curves in MATLAB and LPILE are identical, whereas for sand there are some differences in the results (as discussed above). When handling homogeneous soils consisting of soft or stiff clay the existing MATLAB-script could be used, but for sand additional research might be needed before resorting to MATLAB instead of LPILE.

It should be noted that in the validation above no layered soil has been examined. A typical soil could consist of different types of clay and sand, among other soil types. If many layers are involved in the computation of $P - y$ curves and the layered soil approach is expected to have a large influence on the results, LPILE should be used, especially if some sand layers are present in the studied soil. However, the layered soil approach could be included in the MATLAB-script in the future, leaving LPILE with no advantage over MATLAB. This would lead to LPILE being replaced by MATLAB and thus license money would be saved.

Another benefit with using MATLAB to compute $P - y$ curves is that the user can follow and understand every calculation step to obtain the relationship. If some modifications to the script are needed, such as adding another soil type, this is easily done by the user. This is not true for LPILE and if one identifies some limitations in the program, one might have to resort, in a worst case scenario, to purchasing a license for another geotechnical program, thus increasing the simulation costs.